Digital quantum computation of fermion-boson interacting systems

Alexandru Macridin, Panagiotis Spentzouris, James Amundson, and Roni Harnik
Fermilab, P.O. Box 500, Batavia, Illinois 60510, USA

(Received 25 May 2018; published 9 October 2018)

We introduce a method for representing the low-energy subspace of a bosonic field theory on the qubit space of digital quantum computers. This discretization leads to an exponentially precise description of the subspace of the continuous theory thanks to the Nyquist-Shannon sampling theorem. The method makes the implementation of quantum algorithms for purely bosonic systems as well as fermion-boson interacting systems feasible. We present algorithmic circuits for computing the time evolution of these systems. The complexity of the algorithms scales polynomially with the system size. The algorithm is a natural extension of the existing quantum algorithms for simulating fermion systems in quantum chemistry and condensed-matter physics to systems involving bosons and fermion-boson interactions and has a broad variety of potential applications in particle physics, condensed matter, etc. Due to the relatively small amount of additional resources required by the inclusion of bosons in our algorithm, the simulation of electron-phonon and similar systems can be placed in the same near-future reach as the simulation of interacting electron systems. We benchmark our algorithm by implementing it for a two-site Holstein polaron problem on an Atos Quantum Learning Machine quantum simulator. The polaron quantum simulations are in excellent agreement with the results obtained by exact diagonalization.

DOI: 10.1103/PhysRevA.98.042312

I. INTRODUCTION

Recent advances in quantum hardware technology have initiated a new era in computing science. As quantum hardware has advanced, the development of quantum algorithms has become an area of intensive research. Quantum computers are naturally suited to simulate the evolution of quantum systems. For example, the algorithms for simulating fermion systems in quantum chemistry and condensed matter physics have proven to be especially successful [1–9]. Due to the relatively small amount of resources required, optimized fermion algorithms are very promising for near-future quantum simulations. Unfortunately, purely fermionic models preclude the simulation of physically important theories with bosonic degrees of freedom such as phonons, photons, and gluons, which appear in condensed-matter and high-energy physics. In this paper we extend the existing fermion algorithms to include bosons, opening up the possibility for quantum simulation to whole new classes of physical systems.

This paper addresses nonrelativistic fermion-boson quantum field theories with focus on electron-phonon systems. The interaction of electrons with other bosonic collective excitations in solids (such as spin, orbital, charge, etc.) can be addressed by models similar to the electron-phonon model. We address both fermion-boson and boson-boson interactions. Our algorithm can also be applied to quantum optics problems. Since the quantum simulation of relativistic field theories is as an important goal for high-energy physics, we consider this approach as a first step towards that direction.

While there are established ways to map fermion states to qubits [3,6,10], the literature contains fewer discussions on representing bosons on gate quantum computers. As discussed in Ref. [11], bosons can be represented as a sum of n_x parafermions (qubits), up to an error $O(n/n_x)$, where n is the boson state occupation number. This representation requires a large number of qubits, especially in the intermediate and strong coupling regimes where n is large. In addition, no algorithm has been proposed to describe the evolution of boson states in this representation. In Refs. [5,12] purely bosonic systems with a fixed number of bosons are addressed, but the method is not suitable for fermion-boson interacting systems where the number of bosons is not conserved. An algorithm for calculating scattering amplitudes in quantum field theories has been proposed in Ref. [13]. Their approach is based on the discretization of the continuous field value at each lattice site. The required number of qubits per lattice site scales as $\log(1/\epsilon)$, where ϵ is the desired accuracy. Our algorithm also relies on field discretization, but the number of qubits per lattice site needed to represent the bosons scales exponentially faster, $\approx \log[\log(1/\epsilon)]$. In fact, when our algorithm is applied to electron-phonon models, we find that only a small number of additional qubits per site, $n_x \approx 6$ or 7, is enough to simulate phonons with exponentially good accuracy in most problems of physical interest, including the weak, intermediate, and strong coupling regimes.

It is worth mentioning that the quantum computation of interacting fermion-boson systems has been addressed in trapped ion systems [14–17]. In these cases, the bosonic states were mapped to the ions' vibrational states. However, this method is specific to the particular kind of hardware used, which possesses additional degrees of freedom (i.e., vibrational states of ions) in addition to qubits; the additional degrees of freedom were used for the boson representation. Our approach to quantum computation of systems with bosons is different since we consider boson representation solely on qubits.

The representation of the boson space on qubits is the most important result of this work. This representation

allows an efficient simulation of the evolution operator of the fermion-boson systems. The bosonic degrees of freedom are treated as a finite set of harmonic oscillators. We show that the low-energy space of a harmonic oscillator is, up to an exponentially small error, isomorphic with the low-energy subspace of a finite-sized Hilbert space. The finite-sized boson Hilbert space is mapped onto the qubit space of universal quantum computers. The size of the low-energy subspace is given by the maximum boson-number cutoff; the finite size of the Hilbert space increases linearly with this cutoff. The number of qubits necessary to store the bosons scales logarithmically with the cutoff.

Our method for truncating the harmonic oscillator space can also be applied to simulate the Schrödinger equation on a quantum computer. A similar finite-sized Hilbert space truncation is employed by the Fourier grid Hamiltonian (FGH) method [18] and is related to more general discrete variable representation (DVR) methods [19–21]. We present an explanation for the exponential accuracy of the FGH method based on the Nyquist-Shannon sampling theorem [22].

The fermions in our algorithm are mapped to qubit states via the Jordan-Wigner transformation [3,6,23]. Quantum algorithms for interacting fermions have been addressed at length in numerous papers; see for example Refs. [4,6,7]. The evolution of the pure-fermion Hamiltonian is not addressed here. We present algorithmic circuits for the evolution of the pure-boson Hamiltonian and the fermion-boson interacting Hamiltonian. The additional qubits needed to accommodate bosons is $O(Nn_x)$ where N is the number of harmonic oscillators, which scales linearly with the system size, and n_x is the number of qubits per harmonic oscillator, which is independent of N. For long-range m-body boson-boson interactions (i.e., an m-leg interaction vertex), the additional circuit depth is $O(N^m)$. In general long-range fermion-boson interactions yield an additional depth of $O(N^2)$. However, when the bosons couple to the fermion hopping, as happens in electron-phonon models, the additional depth scales as $O(N)$. For finite-range boson-boson and fermion-boson interaction, the additional circuit depth is constant.

As an example of fermion-boson interacting systems, we address the polaron problem [24]. The polaron is a bound state between an electron and its induced crystal lattice deformation; it can be thought of as an electron dressed by phonons. Although it involves only one electron, the polaron problem is nontrivial and in general cannot be solved on classical computers due to the exponential increase of the Hilbert space with increasing system size. Polaronic effects can significantly change the electric and transport properties of materials, angle-resolved photoemission spectra, superconducting properties, etc. We benchmark our algorithm by running a simulation of the two-site Holstein polaron [25], utilizing the quantum phase estimation (QPE) method [2,26–30] on an Atos Quantum Learning Machine (QLM) simulator. The energy and phonon distribution of the polaron state agree with results obtained from exact diagonalization.

The paper is organized as follows. In Sec. II the fermion-boson model is introduced. In Sec. III we address the representation of bosons on a finite-sized space. The quantum algorithm is described in Sec. IV. Section V presents the results of the QPE simulation for the Holstein polaron. In Sec. VI we discuss the general applicability of our approach to physical systems. Summary and conclusions are given in Sec. VII.

II. FERMION-BOSON HAMILTONIAN

In our algorithm, the fermion operators appearing in the Hamiltonian need to be expressed in the second quantized form. On the other hand, the bosonic operators are required to be written as function of the canonical "position" and "momentum" operators X and P, obeying the commutation relation $[X, P] = i$.

In this section we start with the electron-phonon Hamiltonian since it constitutes one of the most common physical examples of nonrelativistic fermion-boson interacting systems. We will follow with a general fermion-boson Hamiltonian written in the second quantized form and will describe the steps necessary to rewrite it in a form suitable for quantum computation.

A. Electron-phonon model

The electron-phonon model describes the electronic and ionic degrees of freedom in a solid. The model can be derived (see Refs. [31–33] for more details) from the Hamiltonian

$$H = \sum_i \frac{p_i^2}{2m} + \sum_{n,\alpha} \frac{P_{n\alpha}^2}{2M_\alpha} + \sum_{i\neq j} V_e(r_i, r_j) + \sum_{n\alpha\neq m\beta} V_p(R_{n\alpha}, R_{m\beta}) + \sum_{i,n\alpha} V_{ep}(r_i, R_{n\alpha}). \quad (1)$$

In Eq. (1) the index i labels the electrons while the index n labels the crystal's unit cells. The ions in the unit cell are labeled by α. The first two terms represent the kinetic energy of the electrons and ions, while the last three terms describe the electron-electron, ion-ion, and electron-ion interactions, respectively.

With the assumption that the ions' motion is characterized only by small displacements around their equilibrium position $R_0 = \{R_{n\alpha 0}\}_{n\alpha}$, Eq. (1) can be written as

$$H = H_e + H_p + H_{ep}, \quad (2)$$

with

$$H_e = \sum_i \frac{p_i^2}{2m} + \sum_i V_{ep}(r_i, R_0) + \sum_{i\neq j} V_e(r_i, r_j), \quad (3)$$

$$H_p = \sum_{n\alpha} \frac{P_{n\alpha}^2}{2M_\alpha} + \sum_{n\alpha,m\beta} \frac{\partial^2 V_p(R_0)}{\partial R_{n\alpha}\partial R_{m\beta}} \Delta R_{n\alpha}\Delta R_{m\beta}, \quad (4)$$

$$H_{ep} = \sum_{i,n\alpha} \frac{\partial V_{ep}(r_i, R_0)}{\partial R_{n\alpha}} \Delta R_{n\alpha}. \quad (5)$$

Since the ions' potential energy is minimum at the equilibrium position R_0, we have taken $\partial V_p(R_0)/\partial R_{n\alpha} = 0$ when deriving Eq. (4).

The term H_e contains only the electronic degrees of freedom and reads as, in the second quantized form,

$$H_e = \sum_{ij} t_{ij}(c_i^\dagger c_j + c_j^\dagger c_i) + \sum_{ijkl} U_{ijkl} c_i^\dagger c_j^\dagger c_k c_l, \quad (6)$$

where $c_i^\dagger$ (c_i) represents the electron creation (annihilation) operator for the state i.

The term H_p describes the ionic vibration and can be written as a sum of coupled harmonic oscillators

$$H_p = \sum_{n\nu} \frac{P_{n\nu}^2}{2M_\nu} + \frac{1}{2} M_\nu \omega_{n\nu}^2 X_{n\nu}^2 + \sum_{n\nu m\mu} K_{n\nu m\mu} X_{n\nu} X_{m\mu}, \quad (7)$$

where ν and μ are vibrational mode labels. The operators $X_{n\nu} = \mathbf{O}(\{\Delta R_{n\alpha}\})$ and $P_{n\nu} = \mathbf{O}(\{P_{n\alpha}\})$ obey the canonical commutation relation $[X_{n\nu}, P_{m\mu}] = i\delta_{nm}\delta_{\nu\mu}$ and are obtained by an orthogonal transformation $\mathbf{O}$ of the vectors $\{\Delta R_{n\alpha}\}$ and $\{P_{n\alpha}\}$, respectively. In general, the vibrational modes are determined by requesting that the Hamiltonian (7) written in the momentum basis reduces to a sum of independent oscillators. Since coupled harmonic oscillators can be easily simulated with our algorithm, for our purpose this decomposition into independent momentum modes is not necessary and in most cases not even optimal. The mode label ν in Eq. (7) represents just a convenient basis choice. The optimal basis is dependent on the particular system under investigation. As will become clear later, the algorithm is efficient in a basis where the interactions have short range and the number of phonons per state is small.

The electron-ion interaction term is

$$H_{ep} = \sum_{ijn\nu} g_{ijn\nu} (c_i^\dagger c_j + c_j^\dagger c_i) X_{n\nu}, \quad (8)$$

and couples single-particle electron operators with ions' position operators.

Note that in the literature, unlike in our representation, both the electron and phonon operators in the electron-phonon Hamiltonians are usually written in the second quantized form.

B. General fermion-boson model

We start with a fermion-boson Hamiltonian written in the second quantized form

$$H = H_f + H_b + H_{fb}, \quad (9)$$

where H_f is the fermion Hamiltonian, as in Eq. (6), H_b contains only bosonic degrees of freedom, and H_{fb} describes the fermion-boson interaction.

1. Boson Hamiltonian

We split the boson Hamiltonian into three parts

$$H_b = H_{b0} + H_{bs} + H_{bi}. \quad (10)$$

The term H_{b0} is noninteracting and is written

$$H_{b0} = \sum_{mn} \xi_{mn} b_m^\dagger b_n + \sum_n (\zeta_n b_n^\dagger + \zeta_n^* b_n). \quad (11)$$

The term H_{bs} is the *squeezing* Hamiltonian [34]; we consider it explicitly since it is of interest in quantum optics. It reads as

$$H_{bs} = \sum_{nm} (\lambda_{nm} b_n^\dagger b_m^\dagger + \lambda_{nm}^* b_n b_m). \quad (12)$$

The Hamiltonian H_{bi} contains interacting terms consisting of a product of three or four creation (or annihilation) operators

$$\begin{aligned} H_{bi} = &\sum_{nmr} U_{nmr} b_n^\dagger b_m^\dagger b_r + \sum_{nmr} V_{nmr} b_n^\dagger b_m^\dagger b_r^\dagger \\ &+ \sum_{nmrs} T_{nmrs} b_n^\dagger b_m^\dagger b_r b_s + \sum_{nmrs} W_{nmrs} b_n^\dagger b_m^\dagger b_r^\dagger b_s \\ &+ \sum_{nmrs} Y_{nmrs} b_n^\dagger b_m^\dagger b_r^\dagger b_s^\dagger + \text{H.c.} \end{aligned} \quad (13)$$

The notation H.c. means Hermitian conjugate and ensures the Hamiltonian (13) is Hermitian. In Eq. (13) we consider the order of the interaction to be at maximum 4 (i.e., allowing for up to 4-leg interaction vertices), as this is relevant for modeling gluon-gluon interactions in quantum chromodynamics. However, higher-order interaction terms can be considered in our algorithm as well.

The boson creation and annihilation operators obey the commutation relations $[b_n, b_m^\dagger] = \delta_{nm}$, $[b_n, b_m] = 0$, and $[b_n^\dagger, b_m^\dagger] = 0$. The following transformation

$$X_n = \frac{1}{\sqrt{2l_n}} W (b_n^\dagger + b_n), \quad (14)$$

$$P_n = i\sqrt{\frac{l_n}{2}} (b_n^\dagger - b_n), \quad (15)$$

where l_n is an arbitrary constant, yields canonical position and momentum operators (which are proportional to quadrature operators in quantum optics), satisfying $[X_n, P_m] = i\delta_{nm}$.

The Hamiltonian H_{b0} becomes

$$\begin{aligned} H_{b0} = &\sum_n \frac{\xi_{nn}}{l_n} \left(\frac{P_n^2}{2} + \frac{l_n^2}{2} X_n^2 - \frac{l_n}{2} \right) \\ &+ \sum_{m<n} \text{Re}\xi_{mn} \left(\frac{P_m P_n}{\sqrt{l_m l_n}} + \sqrt{l_m l_n} X_m X_n \right) \\ &+ \sum_{m<n} \text{Im}\xi_{mn} \left(-\sqrt{\frac{l_n}{l_m}} X_n P_m + \sqrt{\frac{l_m}{l_n}} X_m P_n \right) \\ &+ \sum_n \text{Re}\zeta_n \sqrt{2l_n} X_n + \sum_n \text{Im}\zeta_n \sqrt{\frac{2}{l_n}} P_n. \end{aligned} \quad (16)$$

The Hamiltonian (16), which is analogous to the phonon Hamiltonian (7), consists of a sum of coupled harmonic oscillators. However, unlike Eq. (7) where only coupling of the type $X_n X_m$ between the position operators at different sites is considered, the Hamiltonian (16) also includes coupling terms of type $P_n P_m$ and $X_n P_m$ ($n \neq m$). Besides, the Hamiltonian (16) includes linear coupling of the canonical position and momentum operators to some arbitrary fields $\text{Re}\zeta$ and $\text{Im}\zeta$, respectively.

The squeezing Hamiltonian can be written as

$$\begin{aligned} H_{bs} = &\sum_{n\neq m} -\text{Re}\lambda_{nm} \left(\frac{P_n P_m}{\sqrt{l_n l_m}} - \sqrt{l_n l_m} X_n X_m \right) \\ &+ \sum_{n\neq m} \text{Im}\lambda_{nm} \left(\sqrt{\frac{l_n}{l_m}} X_n P_m + \sqrt{\frac{l_m}{l_n}} P_n X_m \right) \end{aligned}$$

$$+\sum_n -\frac{\mathrm{Re}\lambda_{nn}}{l_n}\left(\frac{P_n^2}{2}-\frac{l_n^2}{2}X_n^2\right)$$
$$+\frac{1}{2}\sum_n \mathrm{Im}\lambda_{nn}(X_nP_n+P_nX_n). \quad (17)$$

As in H_{b0} (16), the Hamiltonian (17) contains terms X_nP_m ($n\neq m$), X_nX_m, and P_nP_m. It also contains local terms X_nP_n which require a different algorithmic implementation, as explained in Sec. IV E.

Employing Eqs. (14) and (15), the Hamiltonian H_{bi} (13) transforms into a sum of terms of type $A_nA_mA_r$ and $A_nA_mA_rA_s$, where A_n is either the X_n or the P_n operator of the harmonic oscillator n.

2. Fermion-boson coupling

We consider a model where the interaction is given by coupling single-particle fermion operators with boson creation and annihilation operators

$$H_{fb}=\sum_{ijn}(g_{ijn}c_i^\dagger c_j b_n^\dagger+g_{ijn}^* c_j^\dagger c_i b_n). \quad (18)$$

After employing Eqs. (14) and (15), H_{fb} becomes

$$H_{fb}=\sum_{ijn}\sqrt{\frac{l_n}{2}}\mathrm{Re}g_{ijn}(c_i^\dagger c_j+c_j^\dagger c_i)X_n \quad (19)$$
$$+\sum_{ijn}\frac{-\mathrm{Im}g_{ijn}}{\sqrt{2l_n}}(c_i^\dagger c_j+c_j^\dagger c_i)P_n \quad (20)$$
$$+\sum_{ijn}i\sqrt{\frac{l_n}{2}}\mathrm{Im}g_{ijn}(c_i^\dagger c_j-c_j^\dagger c_i)X_n \quad (21)$$
$$+\sum_{ijn}\frac{i\,\mathrm{Re}g_{ijn}}{\sqrt{2l_n}}(c_i^\dagger c_j-c_j^\dagger c_i)P_n. \quad (22)$$

The first term above [Eq. (19)] is of the same type as the electron-phonon coupling [Eq. (8)]. The second term [Eq. (20)] represents the coupling of the fermion kinetic energy operator to the boson momentum operator. The last two terms [Eqs. (21) and (22)] describe the coupling of the fermion current operator to the boson position and momentum operators, respectively.

III. BOSON REPRESENTATION ON A FINITE SPACE

The boson operators in our model are the canonical position and momentum operators, as discussed in Sec. II. The bosons are described by a set of coupled harmonic oscillators labeled by state index (for example, the position and vibrational mode indices for phonons). The boson Hilbert space is a direct product of the Hilbert spaces of the harmonic oscillators. In this section, we address the representation of the harmonic oscillator space on a finite-sized space. In Sec. IV we will show how to map this finite-sized space onto the qubit space of a quantum computer.

A. Harmonic oscillator

The harmonic oscillator is described by the Hamiltonian

$$H_h=\tfrac{1}{2}P^2+\tfrac{1}{2}X^2, \quad (23)$$

where the operators X, P, and H_h are rescaled by $1/\sqrt{M\omega}$, $\sqrt{M\omega}$, and $1/\omega$, respectively. The eigenvalues and eigenvectors of H_h are

$$E_n=n+\tfrac{1}{2} \quad (24)$$

and

$$|\phi_n\rangle=\int\phi_n(x)|x\rangle dx=\int\hat{\phi}_n(p)|p\rangle dp, \quad (25)$$

where $\{|x\rangle\}$ is the position coordinate basis and $\{|p\rangle\}$ is the momentum coordinate basis. The eigenfunction

$$\phi_n(x)=\frac{1}{\pi^{\frac{1}{4}}\sqrt{2^n n!}}e^{-\frac{x^2}{2}}H_n(x) \quad (26)$$

is the Hermite-Gauss (HG) function of order n and $\hat{\phi}_n(p)$ is its Fourier transform to the momentum representation.

In addition to being eigenfunctions of the harmonic oscillator Hamiltonian, the HG functions are also eigenfunctions of the Fourier transform operator [35]

$$[\mathcal{F}(\phi_n)](p)\equiv\hat{\phi}_n(p)=(-i)^n\phi_n(p). \quad (27)$$

The HG functions satisfy the relations

$$x\phi_n(x)=\frac{1}{\sqrt{2}}[\sqrt{n+1}\phi_{n+1}(x)+\sqrt{n}\phi_{n-1}(x)] \quad (28)$$

and

$$p\hat{\phi}_n(p)=\frac{i}{\sqrt{2}}[\sqrt{n+1}\hat{\phi}_{n+1}(p)-\sqrt{n}\hat{\phi}_{n-1}(p)]. \quad (29)$$

Equation (28) follows from the recurrence relations of the Hermite polynomials [36], while Eq. (29) can be obtained from Eq. (28) by employing Eq. (27). Note that Eqs. (28) and (29) are just the familiar eigenvalue equations $\langle x|X|\phi_n\rangle=x\langle x|\phi_n\rangle$ and $\langle p|P|\phi_n\rangle=p\langle p|\phi_n\rangle$, respectively, where the position operator $X=(b^\dagger+b)/\sqrt{2}$ and momentum operator $P=i(b^\dagger-b)/\sqrt{2}$ are written as functions of the creation and the annihilation operators $b^\dagger$ and b. Remember that the operators $b^\dagger$ and b satisfy

$$b^\dagger|\phi_n\rangle=\sqrt{n+1}|\phi_{n+1}\rangle, \quad (30)$$

$$b|\phi_n\rangle=\sqrt{n}|\phi_{n-1}\rangle. \quad (31)$$

Equations (28) and (29) together with the exponential decay at large argument, Eqs. (26) and (27), are the essential properties of the HG functions which make the controlled truncation of the Hilbert space discussed in Sec. III B feasible.

B. Discretization of the harmonic oscillator space

In both the coordinate and momentum representations, the HG functions decay exponentially quickly to zero for large arguments. The width of the HG functions, i.e., the interval range enclosing most of the weight $|\phi_n(x)|$, increases with increasing n. For a cutoff number N_{ph} one can define a width $2L$ such that $|\phi_n(x)|\approx 0$ when $|x|>L$ for all $n<N_{ph}$. Equation (27) implies that for the same L, $|\hat{\phi}_n(p)|\approx 0$ when $|p|>L$ and $n<N_{ph}$. The error of these approximations can be made arbitrarily small through a large enough choice of L.

Restricting the problem to the region $|p|<L$, the Nyquist-Shannon sampling theorem [22] for band limited signals

applies. It shows that, without loss of information, $\phi_n(x)$ can be sampled at points $x_i = i\Delta$, where i is an integer and $\Delta = \pi/L$. Moreover, with the same exponentially small error, we can restrict i to N_x points such that $x_i \in [-L, L]$. The HG function can be written as

$$\phi_n(x) = \sum_{i=-\frac{N_x}{2}}^{\frac{N_x}{2}-1} \phi_n(x_i) u_i(x) + O(\epsilon), \tag{32}$$

where $u_i(x) = \mathrm{sinc}(\frac{x-x_i}{\Delta})$. The minimum N_x to satisfy the requirement $x_i \in [-L, L]$ is given by the equation $2L = N_x\Delta$, which implies $2L = \sqrt{2\pi N_x}$ and $\Delta = \sqrt{2\pi/N_x}$ with $i = \overline{-N_x/2, N_x/2-1}$. For a more detailed discussion about the application of the Nyquist-Shannon sampling theorem to the HG functions, see Appendix A.

The properties of the HG functions require that $N_x > N_{ph}$. This can be understood within the framework of the Wentzel-Kramers-Brillouin (WKB) approximation [37] for the harmonic oscillator. The magnitude of $\phi_n(x)$ is exponentially small in the classically forbidden region where $V(x) - E_n > 0$, and enhanced around the turning points defined by $V(x_{tn}) - E_n = 0$. In the harmonic oscillator potential $V(x) = x^2/2$ the turning points are given by $x_{tn} = \pm\sqrt{2n+1}$. The condition $L > |x_{tn}|$ for $n = N_{ph}$ required by the Nyquist-Shannon sampling theorem implies

$$N_x > \left(\frac{4}{\pi} N_{ph} + \frac{2}{\pi}\right), \tag{33}$$

i.e., $N_x > N_{ph}$.

Let us consider the finite-sized subspace $\tilde{\mathcal{H}}$ spanned by the sampling position vectors $\{|x_i\rangle\}_i$ for integer $i = \overline{-N_x/2, N_x/2-1}$, and define the vectors $|\chi_n\rangle \in \tilde{\mathcal{H}}$ by

$$\langle x_i|\chi_n\rangle \equiv \sqrt{\Delta}\phi_n(x_i). \tag{34}$$

Two essential properties of the vectors $|\chi_n\rangle$ with $n < N_{ph}$ are an immediate consequence of the Nyquist-Shannon sampling theorem. First, the vectors $|\chi_n\rangle$ are orthonormal; see Eqs. (A9) and (A10). Second [see Eqs. (A13) and (A14))],

$$\langle p_m|\chi_n\rangle = \sqrt{2\pi\Delta}\hat{\phi}_n(p_m), \tag{35}$$

where the vectors

$$|p_m\rangle = \frac{1}{\sqrt{N_x}} \sum_{i=-\frac{N_x}{2}}^{\frac{N_x}{2}-1} e^{i x_i p_m} |x_i\rangle, \tag{36}$$

with $p_m = m\Delta$ and $m = \overline{-N_x/2, N_x/2-1}$, are obtained by the discrete Fourier transform of the $\{|x_i\rangle\}$ vectors. Equation (34) implies that $\langle x_i|\chi_n\rangle$ is proportional to the HG function $\phi_n(x)$ at the grid points $\{x_i\}$, while Eq. (35) implies that its discrete Fourier transform $\langle p_m|\chi_n\rangle$ is proportional to the HG functions in the momentum representation $\hat{\phi}_n(p)$ at the grid points $\{p_m\}$. Therefore, employing Eqs. (28) and (29), one gets

$$x_i\langle x_i|\chi_n\rangle = \frac{1}{\sqrt{2}}(\sqrt{n+1}\langle x_i|\chi_{n+1}\rangle + \sqrt{n}\langle x_i|\chi_{n-1}\rangle), \tag{37}$$

$$p_m\langle p_m|\chi_n\rangle = \frac{i}{\sqrt{2}}(\sqrt{n+1}\langle p_m|\chi_{n+1}\rangle - \sqrt{n}\langle p_m|\chi_{n-1}\rangle). \tag{38}$$

Now, we define the discrete position and momentum operators acting on $\tilde{\mathcal{H}}$ by

$$\tilde{X}|x_i\rangle = x_i|x_i\rangle, \tag{39}$$

$$\tilde{P}|p_m\rangle = p_m|p_m\rangle. \tag{40}$$

Equations (37) and (38) can be written as

$$\tilde{X}|\chi_n\rangle = \frac{1}{\sqrt{2}}(\sqrt{n+1}|\chi_{n+1}\rangle + \sqrt{n}|\chi_{n-1}\rangle), \tag{41}$$

$$\tilde{P}|\chi_n\rangle = \frac{i}{\sqrt{2}}(\sqrt{n+1}|\chi_{n+1}\rangle - \sqrt{n}|\chi_{n-1}\rangle), \tag{42}$$

which implies that

$$[\tilde{X}, \tilde{P}]|\chi_n\rangle = i|\chi_n\rangle \quad \text{for} \quad n < N_{ph}. \tag{43}$$

If we restrict to the subspace spanned by the orthogonal vectors $\{|\chi_n\rangle\}_{n<N_{ph}}$,

$$[\tilde{X}, \tilde{P}] = i, \tag{44}$$

and the algebra generated by $\tilde{X}$ and $\tilde{P}$ is isomorphic with the algebra generated by X and P on the harmonic oscillator subspace spanned by the HG functions $\{|\phi_n\rangle\}_{n<N_{ph}}$. One can also define annihilation and creation operators on $\tilde{\mathcal{H}}$ as

$$\tilde{b}^\dagger = \frac{1}{\sqrt{2}}(\tilde{X} - i\tilde{P}), \ \tilde{b} = \frac{1}{\sqrt{2}}(\tilde{X} + i\tilde{P}), \tag{45}$$

which satisfy

$$[\tilde{b}, \tilde{b}^\dagger] = 1 \tag{46}$$

on the subspace $\{|\chi_n\rangle\}_{n<N_{ph}}$.

On the subspace $\{|\chi_n\rangle\}_{n<N_{ph}}$ the discrete Hamiltonian

$$\tilde{H}_h = \tfrac{1}{2}\tilde{P}^2 + \tfrac{1}{2}\tilde{X}^2 \tag{47}$$

corresponds to the harmonic oscillator Hamiltonian (23). Therefore, $\{|\chi_n\rangle\}_{n<N_{ph}}$ are eigenvectors of $\tilde{H}_h$ with the eigenspectrum $\tilde{H}_h|\chi_n\rangle = (n+1/2)|\chi_n\rangle$. Moreover, $\{|\chi_n\rangle\}_{n<N_{ph}}$ span the low-energy subspace of $\tilde{\mathcal{H}}$, which we will demonstrate by numerically calculating the N_x eigenvalues and eigenvectors of $\tilde{H}_h$.

C. Numerical investigation of the discrete space

The energy spectrum $\tilde{E}_n$ of $\tilde{H}_h$ [Eq. (47)] calculated by exact diagonalization is shown in Fig. 1(a) for two cases, $N_x = 64$ and 128, respectively. A cutoff number N_{ph} can be defined such that the first N_{ph} energy levels are, within a small error, close to the ones corresponding to harmonic oscillator energy levels, i.e., $\tilde{E}_n = E_n + \epsilon$. We will show later in this section that the error ϵ decreases exponentially by increasing N_x or by decreasing N_{ph}.

The low-energy eigenstates $\{|\tilde{\phi}_n\rangle\}_{n<N_{ph}}$ of $\tilde{H}_h$ are the projected HG functions on the discrete basis $\{|\chi_n\rangle\}_{n<N_{ph}}$ [Eq. (34)] in agreement with the theoretical arguments discussed in Sec. III B. This can be inferred from Fig. 1(b), where we see that the overlap $|\langle\tilde{\phi}_n|\chi_n\rangle| = 1 - \epsilon$ for $n < N_{ph}$. The eigenstates $\{|\tilde{\phi}_n\rangle\}$ are calculated by exact diagonalization. Unlike the low-energy states characterized by large probability at small x_i and exponentially small probability density at the grid

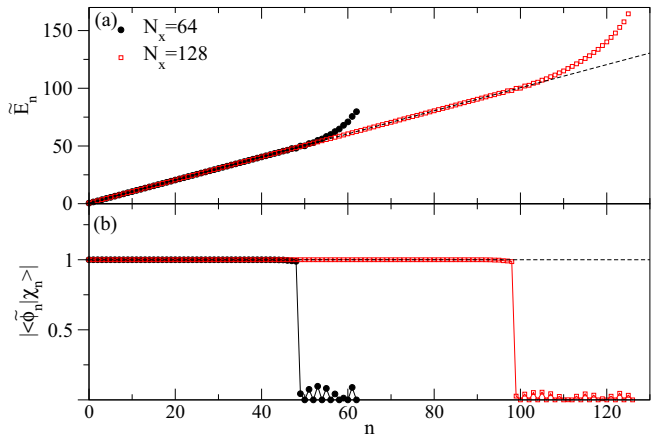

FIG. 1. (a) Energy spectrum $\tilde{E}_n$ of the discrete Hamiltonian $\tilde{H}_h$ [Eq. (47)] for $N_x = 64$ and 128. The dashed line is the continuous harmonic oscillator spectrum [Eq. (24)]. (b) Overlap between the eigenvectors $|\tilde{\phi}_n\rangle$ of $\tilde{H}_h$, and the HG functions projected on the $\{|x_i\rangle\}$ subspace $|\chi_n\rangle$ [Eq. (34)]. For $n < N_{ph}$ where N_{ph} is a cutoff number increasing with increasing N_x, $\tilde{E}_n \approx n + \frac{1}{2}$ and $|\tilde{\phi}_n\rangle \approx |\chi_n\rangle$.

edge (i.e., when $x_i \approx \pm L$), the eigenstates in the high-energy sector $\{|\tilde{\phi}_n\rangle\}_{N_{ph} \leqslant n < N_x}$ have small probability density at small x_i and large probability density close to the grid edge (not shown). They have a small overlap with the projected HG functions, as Fig. 1(b) shows.

Figure 2 shows that $|([\tilde{X}, \tilde{P}] - i)|\tilde{\phi}_n\rangle| < \epsilon$ for $n < N_{ph}$. The value of ϵ is exponentially small and it is a consequence of cutting the tails of the HG functions for $|x|, |p| > L$. Numerically, we find the convergence rate to be

$$\epsilon \lesssim 10 e^{-(0.51 N_x - 0.765 N_{ph})}. \tag{48}$$

We conclude that the numerical calculations agree with the analytical predictions, supporting the isomorphism between

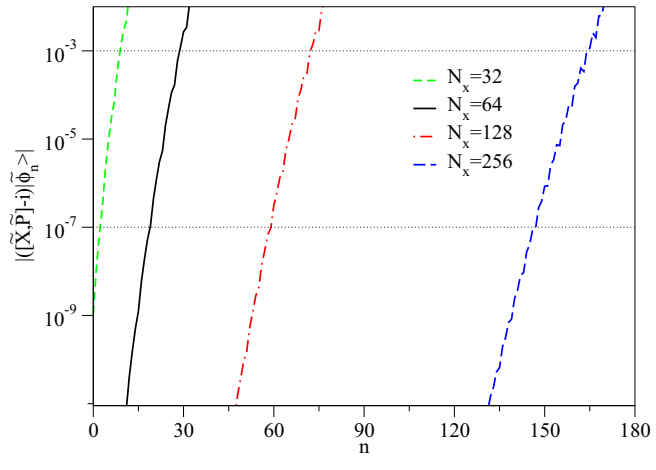

FIG. 2. $|([\tilde{X}, \tilde{P}] - i)|\tilde{\phi}_n\rangle|$ versus n for different values of N_x. For $n < N_{ph}$, the commutation operator satisfies $|([\tilde{X}, \tilde{P}] - i)|\tilde{\phi}_n\rangle| < \epsilon$, with $\epsilon \lesssim 10 \exp[-(0.51 N_x - 0.765 N_{ph})]$. Up to an exponentially small error, the algebra generated by $\{\tilde{X}, \tilde{P}\}$ on the low-energy subspace $\{|\tilde{\phi}_n\rangle\}_{n<N_{ph}}$ of $\tilde{\mathcal{H}}$ is isomorphic with the algebra generated by $\{X, P\}$ on low-energy subspace of the harmonic oscillator $\{|\phi_n\rangle\}_{n<N_{ph}}$.

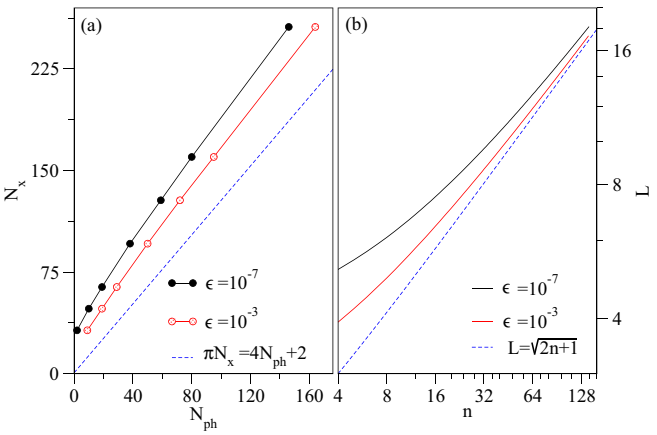

FIG. 3. (a) The size of the discrete space N_x increases linearly with the size of the low-energy subspace N_{ph}. The full (open) symbols are extracted from Fig. 2 for $\epsilon = 10^{-7}$ ($\epsilon = 10^{-3}$). The dashed line is the limit given by the WKB turning points, Eq. (33). (b) (Logarithmic scale) L, the half-width of the HG functions ϕ_n, defined by $1 - \int_{-L}^{L} |\phi_n(x)|^2 dx = \epsilon$ as a function of n. L scales approximately as $\sqrt{n}$. The dashed line corresponds to the WKB equation for the turning points $L = \sqrt{2n+1}$.

the $\{\tilde{X}, \tilde{P}\}$ and the $\{X, P\}$ generated algebras on the low-energy subspace defined by $n < N_{ph}$.

The size N_x of the discrete Hilbert space $\tilde{\mathcal{H}}$ required to accommodate N_{ph} low-energy states increases approximately linearly with increasing N_{ph}. For example, in Fig. 3(a) we plot the minimum N_x necessary to have N_{ph} states in the low-energy regime with $\epsilon = 10^{-7}$ and 10^{-3} accuracy. The proportionality between N_x and N_{ph} can be understood by noticing that the exponential convergence occurs when the grid points x_i cover the width $2L_{N_{ph}}$ of $\phi_{N_{ph}}(x)$. As shown in Fig. 3(b), to a first approximation, $L_{N_{ph}} \propto \sqrt{N_{ph}}$, which is not surprising taking into account that the turning points in the WKB approximation are defined by $\sqrt{2N_{ph}+1}$ [see the discussion before Eq. (33)]. On the other hand, the width covered by N_x points is $\sqrt{2\pi N_x}$, thus being proportional to $\sqrt{N_x}$ and implying linear dependence of $N_x(N_{ph})$.

D. Cutoff of the maximum boson occupation number

As long as the physical problem of interest can be addressed by truncating the number of bosons per state our representation is suitable for quantum computation. In most cases, the boson distribution number is Poissonian, falling exponentially fast to zero with increasing the number of bosons. For electron-phonon systems the cutoff on the maximum phonon occupation number depends on the effective strength of the interaction, on the size of the low-energy space under consideration, and on the desired precision, as discussed below.

In order to understand the truncation of the boson space, let us focus on a particular harmonic oscillator. The states belonging to the chosen harmonic oscillator space evolve under the action of a forced harmonic oscillator Hamiltonian, i.e., a harmonic oscillator with a displacing force. The effective force is determined by the configuration of the fermions and the bosons coupling to the oscillator.

For example, let us consider the electron-phonon system (2), and focus on the harmonic oscillator labeled $n\nu$. The Hamiltonian can be written as

$$H = H_{n\nu} + FX_{n\nu} + BX_{n\nu} + H_1, \tag{49}$$

where

$$H_{n\nu} = \frac{P_{n\nu}^2}{2M_\nu} + \frac{1}{2}M_\nu\omega_{n\nu}^2 X_{n\nu}^2, \tag{50}$$

$$FX_{n\nu} = \left[\sum_{ij} g_{ijn\nu}(c_i^\dagger c_j + c_j^\dagger c_i)\right] X_{n\nu}, \tag{51}$$

$$BX_{n\nu} = \left[\sum_{m\mu\neq n\nu} K_{m\mu n\nu} X_{m\mu}\right] X_{n\nu}. \tag{52}$$

H_1 contains the remaining terms in the Hamiltonian which do not act on the Hilbert space of the harmonic oscillator $n\nu$. Let us consider an arbitrary state $|\Phi\rangle$ which we write as

$$|\Phi\rangle = \sum_{\alpha\beta s} c_{\alpha\beta s}|f_\alpha\rangle \otimes |b_\beta\rangle \otimes |s\rangle_{n\nu}, \tag{53}$$

where $|f_\alpha\rangle \otimes |b_\beta\rangle \otimes |s\rangle_{n\nu}$ form a complete basis set. In Eq. (53), the vectors $|f_\alpha\rangle$ span the electron Hilbert space while the vectors $|b_\beta\rangle \otimes |s\rangle_{n\nu}$ span the full phonon space. The vectors $|s\rangle_{n\nu}$ belong to the Hilbert space of the harmonic oscillator $n\nu$. We choose the vectors $|f_\alpha\rangle$ such that they are eigenvectors of F, i.e., $F|f_\alpha\rangle = f_\alpha|f_\alpha\rangle$, and the vectors $|b_\beta\rangle$ such that they are eigenvectors of B, i.e., $B|b_\beta\rangle = b_\beta|b_\beta\rangle$. Let us now imagine a path integral or Trotter-Suzuki expansion [38,39] of the evolution operator in small time steps. The evolution operator for a small time step θ is

$$\begin{aligned} e^{-i\theta H}|\Phi\rangle &\approx e^{-i\theta H_1} e^{-i\theta(H_{n\nu}+FX_{n\nu}+BX_{n\nu})}|\Phi\rangle \\ &= \sum_{\alpha\beta s} c_{\alpha\beta s}(e^{-i\theta H_1}|f_\alpha\rangle \otimes |b_\beta\rangle) \\ &\quad \otimes (e^{-i\theta[H_{n\nu}+(f_\alpha+b_\beta)X_{n\nu}]}|s\rangle_{n\nu}). \end{aligned} \tag{54}$$

From Eq. (54) one can see that the evolution operator of a full electron-phonon system implies a superposition of forced harmonic Hamiltonians $H_{n\nu} + g_{\alpha\beta}X_{n\nu}$ acting on the phonon space $n\nu$ at every time step. The coupling strength at that particular time step, $g_{\alpha\beta} = f_\alpha + b_\beta$, depends on the configuration α of the electrons interacting with the harmonic oscillator $n\nu$ and the configuration β of the phonons interacting with the harmonic oscillator $n\nu$.

The forced harmonic oscillator problem can be solved exactly [37]. (See also Appendix B.) It turns out that the low-energy space of the forced harmonic oscillator can be obtained from the low-energy space of the unperturbed harmonic oscillator via displacement operators.

Let us assume first that the coupling $g_{\alpha\beta}$ is constant. In that case the forced harmonic oscillator is just a harmonic oscillator with a displaced equilibrium position

$$\begin{aligned} H_g &= \frac{P^2}{2M} + \frac{1}{2}M\omega^2 X^2 + gX \\ &= \frac{P^2}{2M} + \frac{1}{2}M\omega^2\left(X + \frac{g}{M\omega^2}\right)^2 - \frac{g^2}{M\omega^2}. \end{aligned} \tag{55}$$

The term $-g^2/M\omega^2$ is a constant which represents the deformation energy. The eigenstates $\{|\phi_{gn}\rangle\}$ of H_g are obtained by applying the displacement operator [see Eq. (B1)]

$$e^{iP\frac{g}{M\omega^2}} = D\left(-\frac{g}{\omega\sqrt{2M\omega}}\right) = e^{-\frac{g}{\omega\sqrt{2M\omega}}(b^\dagger - b)} \tag{56}$$

on the unperturbed harmonic oscillator H_0 eigenstates $\{|\phi_n\rangle\}$,

$$|\phi_{gn}\rangle = D\left(-\frac{g}{\omega\sqrt{2M\omega}}\right)|\phi_n\rangle, \tag{57}$$

i.e., $\{|\phi_{gn}\rangle\}$ are *displaced number states* [Eq. (B12)].

In general, $g_{\alpha\beta}$ is not constant since it depends on the configuration of the surrounding fermions and bosons interacting with the oscillator, and these surroundings change at every time step. The evolution of a displaced number state $|n, z\rangle \equiv D(z)|\phi_n\rangle$ under the action of the forced harmonic oscillator Hamiltonian with time-dependent force $g_{\alpha\beta}(t)$ is given by [see Eqs. (B20) and (B24)]

$$U(t)|n, z\rangle = e^{i\gamma}e^{i(\delta - n\omega t)}|n, [\zeta_{\alpha\beta}(t) + z]e^{-i\omega t}\rangle, \tag{58}$$

where γ and δ are real phases and $\zeta_{\alpha\beta}(t)$ is

$$\zeta_{\alpha\beta}(t) = -\frac{i}{\sqrt{2M\omega}}\int_0^t g_{\alpha\beta}(u)e^{i\omega u}du. \tag{59}$$

Thus, at any time the evolution of a displaced number state is a displaced number state. Therefore, an initial low-energy state written as a linear combination of displaced number states will remain a linear combination of displaced number states.

As discussed in Appendix B, the boson occupation number of a displaced number state is Poissonian and falls exponentially to zero with increasing boson number. As long as the displacements are bounded, one can chose a cutoff value N_{ph} for truncating the boson Hilbert space to the desired accuracy. Equation (B27) implies that

$$N_{ph} = O(\sqrt{\ln(\epsilon^{-1})}), \tag{60}$$

$$N_{ph} = O(|\zeta_{\max}|^2), \tag{61}$$

$$N_{ph} = O(N_E), \tag{62}$$

where ϵ is the accuracy, N_E is the size of the low-energy space under consideration, and $|\zeta_{\max}| = \max_{t,\alpha,\beta}|\zeta_{\alpha,\beta}(t)|$ is the maximum displacement of the harmonic oscillator under the action of the effective force. Since the maximum displacement is proportional to the coupling $g_{\alpha\beta}$ [see Eq. (59)], one can regard $|\zeta_{\max}|^2$ as the effective coupling strength between the harmonic oscillator and the environment.

Note that the displacement is not bounded if the system is unstable (and $g_{\alpha\beta}$ is unbounded) or when $g_{\alpha\beta}(t)$ is resonant with the oscillator and $\zeta_{\alpha\beta}(t)$ grows linearly with time [see Eq. (59)].

IV. ALGORITHM

Our algorithm simulates the evolution operator e^{-itH} of the fermion-boson systems on a gate quantum computer. As in the fermion algorithms, we employ the Trotter-Suzuki expansion [38,39] of the evolution operator to a product of

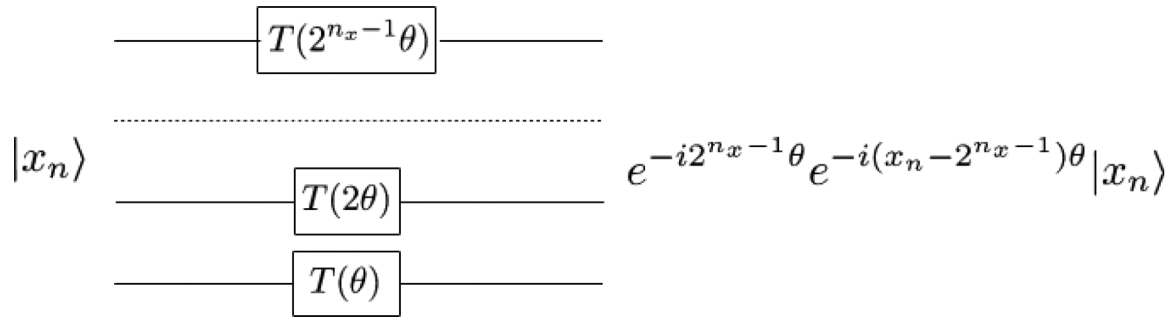

FIG. 4. The circuit for $e^{-i\theta\tilde{X}_n}|x_n\rangle$. On each qubit, a phase shift gate is applied. The angles of the phase shift gates are determined by writing $x_n = \sum_{r=0}^{n_x-1} x_n^r 2^r$, where $\{x_n^r\}_{r=\overline{0,n_x-1}}$ takes binary values. A phase factor $\exp(-i2^{n_x-1}\theta)$ accumulates at every Trotter step.

short-time evolution operators corresponding to the noncommuting terms in the Hamiltonian. For a Hamiltonian written as $H = \sum_m H_m$, the first-order Trotter decomposition reads as

$$e^{-iH\Delta t} = \prod_m e^{-iH_m\Delta t} + O(\Delta t^2). \tag{63}$$

Higher-order decomposition schemes can be used for optimal performance, but that type of optimization is not addressed in this paper. Our main focus is presenting algorithmic circuits for the small time-evolution operators corresponding to the terms in the fermion-boson Hamiltonian.

While the polaron example presented in Sec. V below is based on the QPE method, our algorithm can be utilized using other techniques such as the variational quantum eigensolver (VQE) [8,9] and adiabatic state preparation [40].

A. Qubit representation of harmonic oscillator space

On a gate quantum computer each harmonic oscillator state is represented as a superposition of $N_x = 2^{n_x}$ discrete states $\{|x_j\rangle\}$ and stored in a register of n_x qubits:

$$|\phi\rangle = \sum_{j=0}^{2^{n_x}-1} \phi_j |x_j\rangle. \tag{64}$$

The operators X and P acting on the boson space are replaced by their discrete versions $\tilde{X}$ [Eq. (39)] and $\tilde{P}$ [Eq. (40)], respectively. The states $\{|x_j\rangle\}$ are eigenvectors of $\tilde{X}$. Since the number stored in the register $|x_j\rangle$ in Eq. (64) is between 0 and $N_x - 1$, the eigenvalues x_j,

$$\tilde{X}|x_j\rangle = x_j|x_j\rangle, \tag{65}$$

are

$$x_j = (j - N_x/2)\Delta, \quad j = \overline{0, N_x - 1}. \tag{66}$$

The states $\{|p_n\rangle\}$ obtained via discrete Fourier transform (or quantum Fourier transform) from the states $\{|x_j\rangle\}$,

$$|p_n\rangle = \frac{1}{\sqrt{N_x}} \sum_{j=0}^{N_x-1} e^{i\frac{2\pi}{N_x}jn}|x_j\rangle, \quad n = \overline{0, N_x - 1} \tag{67}$$

are eigenvectors of $\tilde{P}$. Nevertheless, the states $\{|p_n\rangle\}$ in Eq. (67) are different from the ones defined by Eq. (36) since in Eq. (67) the Fourier transform is not centered. As a consequence one has

$$\tilde{P} = p_n|p_n\rangle, \tag{68}$$

with

$$p_n = n\Delta, \quad n = \overline{0, N_x/2 - 1} \tag{69}$$

$$p_n = (n - N_x)\Delta, \quad n = \overline{N_x/2, N_x - 1}. \tag{70}$$

B. Noninteracting boson Hamiltonian

In this section we discuss the implementation of the evolution operators corresponding to the different terms in the noninteracting boson Hamiltonian (16). Unlike the notation used in Sec. IV A where the index j in $|x_j\rangle$ (or n in $|p_n\rangle$) was used to label the basis states of a single harmonic oscillator, here and in the following sections a vector $|x_n\rangle$ represents a state of the harmonic oscillator n (n is a site label).

A circuit for the term

$$e^{-i\theta\tilde{X}_n}|x_n\rangle \tag{71}$$

is shown in Fig. 4. The factor Δ [see Eq. (66)] is absorbed into the definition of θ. On every qubit belonging to the boson register $|x_n\rangle$ a controlled phase shift gate

$$T(\theta_r) = \begin{bmatrix} 1 & 0 \\ 0 & e^{-i\theta_r} \end{bmatrix} \tag{72}$$

with $\theta_r = 2^r\theta$ is applied. Here, r represents the qubit index defined by the binary representation of x_n, i.e., $x_n = \sum_{r=0}^{n_x-1} x_n^r 2^r$, with $\{x_n^r\}_{r=\overline{0,n_x-1}}$ taking binary values. The $N_x/2$ term entering in Eq. (66) yields a phase factor equal to $\exp(-i2^{n_x-1}\theta)$ which accumulates to the wave function at each Trotter step. This phase factor can be tracked classically.

The implementation of

$$e^{-i\theta\tilde{X}_n^2}|x_n\rangle \tag{73}$$

requires phase shift gates and is shown in Fig. 5. Note that, unlike the circuit for Eq. (71), the circuit for Eq. (73) requires extra $n_x(n_x - 1)/2$ controlled phase shift gates, a consequence of squaring x_n. The angles for the phase shift gates are determined by writing $(x_n - N_x/2)^2$ in the binary format (see the figure's caption).

The evolution operator

$$e^{-i\theta\tilde{X}_n\tilde{X}_m}|x_n\rangle|x_m\rangle \tag{74}$$

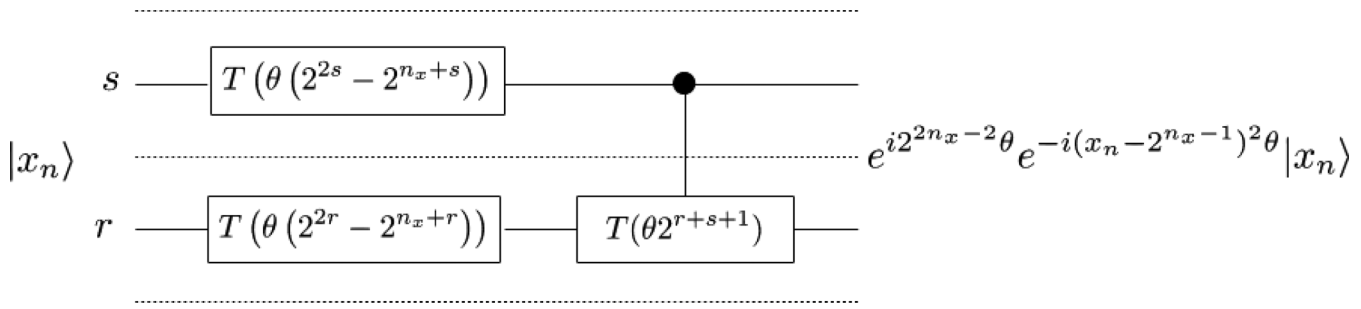

FIG. 5. The circuit for $e^{-i\theta\tilde{X}_n^2}|x_n\rangle$ requires n_x phase shift gates (one on each qubit) and $n_x(n_x-1)/2$ controlled phase shift gates. The angles of the phase shift gates are determined by writing $(x_n-2^{n_x-1})^2=\sum_{r=0}^{n_x-1}x_n^r(2^{2r}-2^{n_x+r})+\sum_{r<s}x_n^r x_n^s 2^{r+s+1}+2^{2n_x-2}$, where $\{x_n^r\}_{r=\overline{0,n_x-1}}$ is the binary representation of x_n, i.e., $x_n=\sum_{r=0}^{n_x-1}x_n^r 2^r$. A phase factor $\exp(i2^{n_x-2}\theta)$ accumulates at every Trotter step.

describes the coupling between oscillators n and m and requires two boson registers, as shown in Fig. 6. The circuit is similar to the ones for Eqs. (71) and (73), consisting in phase shift gates. The phase shift angles are determined by writing the product $(x_n-N_x/2)(x_m-N_x/2)$ as a sum with binary coefficients (see the figure's caption). The circuit reduces to n_x^2 controlled phase shift gates and $2n_x$ phase shift gates.

For the implementation of $e^{-i\theta\tilde{P}_n}|x_n\rangle$, $e^{-i\theta\tilde{P}_n^2}|x_n\rangle$, and $e^{-i\theta\tilde{P}_n\tilde{X}_m}|x_n\rangle|x_m\rangle$ $(n\neq m)$, one first applies a quantum Fourier transform (QFT) [29] $|x_n\rangle\xrightarrow{\text{QFT}}|p_n\rangle$. Then, $e^{-i\theta\tilde{P}_n}|p_n\rangle$, $e^{-i\theta\tilde{P}_n^2}|p_n\rangle$, and $e^{-i\theta\tilde{P}_n\tilde{X}_m}|p_n\rangle|x_m\rangle$ are implemented by circuits similar to the ones shown in Figs. 4, 5, and 6, respectively. These circuits contain phase shift gates with angles determined by writing the eigenvalues of the operators $\tilde{P}_n$, $\tilde{P}_n^2$, and $\tilde{P}_n\tilde{X}_m$ in binary representation. The last step is an inverse QFT $|p_n\rangle\xrightarrow{\text{IQFT}}|x_n\rangle$. The idea of implementing the Hamiltonian terms which are functions of the momentum operator by going to the momentum basis and back via Fourier transform was first discussed in Refs. [41,42].

The implementation of $e^{-i\theta\tilde{P}_n\tilde{P}_m}|x_n\rangle|x_m\rangle$ requires two QFT transforms of the $|x_n\rangle$ and $|x_m\rangle$ registers, such that $|x_n\rangle|x_m\rangle\xrightarrow{\text{QFT}}|p_n\rangle|p_m\rangle$. The operator $e^{-i\theta\tilde{P}_n\tilde{P}_m}|p_n\rangle|p_m\rangle$ is implemented in an analogous way to the one shown in Fig. 6. The circuit ends with two inverse QFT transforms $|p_n\rangle|p_m\rangle\xrightarrow{\text{IQFT}}|x_n\rangle|x_m\rangle$.

C. Fermion Hamiltonian

The algorithm for fermions is described at length in numerous papers (see, for example, Refs. [4,6,7].) We assume here an implementation which requires Jordan-Wigner mapping of the fermion operators to the Pauli operators X, Y, and Z as in

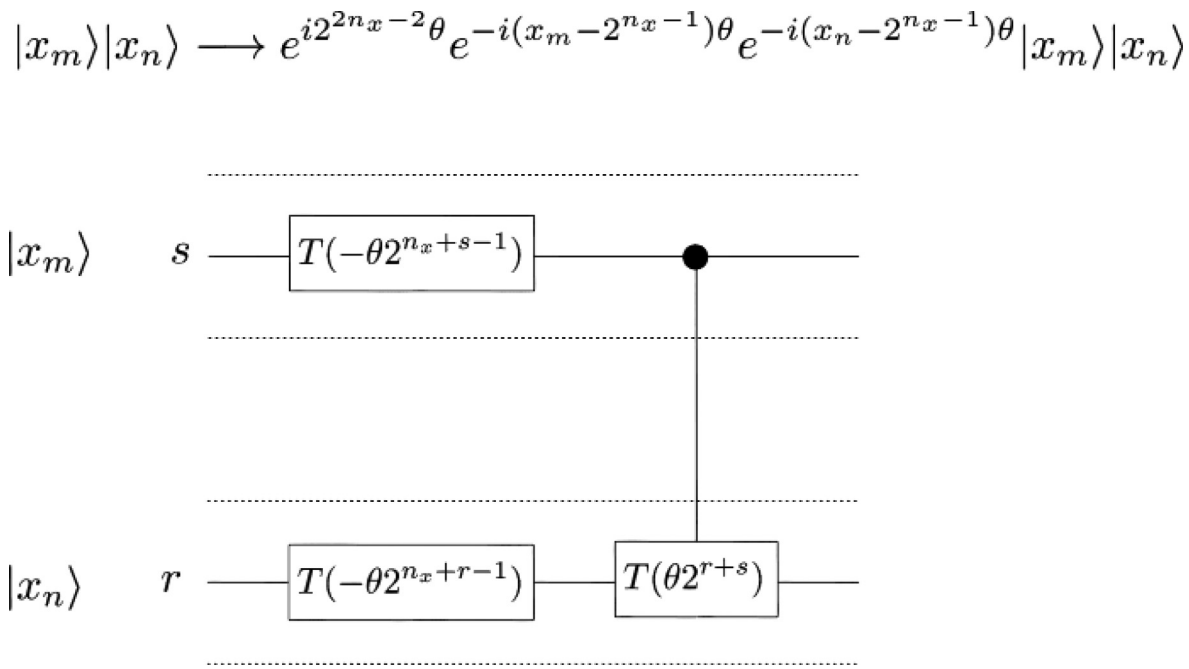

FIG. 6. The circuit for $e^{-i\theta\tilde{X}_n\tilde{X}_m}|x_n\rangle|x_m\rangle$ requires $2n_x$ phase shift gates (one on each qubit of the two boson registers) and n_x^2 controlled phase shift gates. The angles of the phase shift gates are determined by writing $(x_n-2^{n_x-1})(x_m-2^{n_x-1})=\sum_{r,s=0}^{n_x-1}x_n^r x_m^s 2^{r+s}-\sum_{r=0}^{n_x-1}(x_n^r+x_m^r)2^{r+n_x-1}+2^{2n_x-2}$, where $\{x_n^r\}_{r=\overline{0,n_x-1}}$ is the binary representation of x_n, i.e., $x_n=\sum_{r=0}^{n_x-1}x_n^r 2^r$. A phase factor $\exp(i2^{n_x-2}\theta)$ accumulates at every Trotter step.

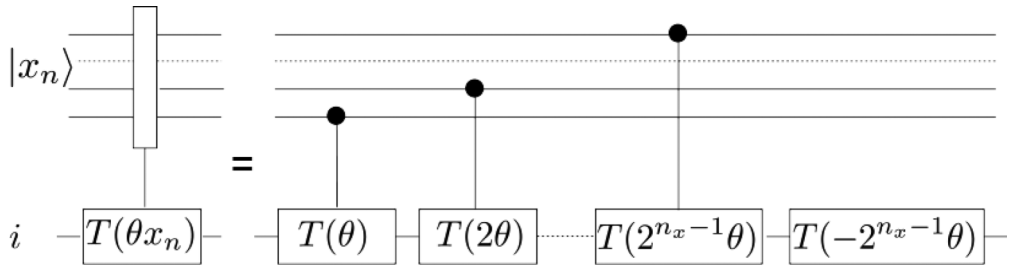

FIG. 7. Circuit describing $e^{-i\theta c_i^\dagger c_i \tilde{X}_n}|i\rangle \otimes |x_n\rangle$. The phase shift angle is proportional to the boson coordinate $x_n - 2^{n_x-1} = \sum_{r=0}^{n_x-1} x_n^r 2^r - 2^{n_x-1}$, where $\{x_n^r\}_{r=\overline{0,n_x-1}}$ take binary values.

Ref. [7]. Each fermion orbital requires a qubit. The qubit state $|\uparrow\rangle \equiv |0\rangle$ corresponds to an unoccupied fermion orbital, while the qubit state $|\downarrow\rangle \equiv |1\rangle$ corresponds to an occupied orbital.

D. Fermion-boson interaction Hamiltonian

The interaction Hamiltonian acts on both the fermion and boson parts of the Hilbert space and involves coupling between single-particle fermion operators and the boson X or P operators, as described by Eqs. (19), (20), (21), and (22).

The expressions for the single-particle fermion operators as functions of the Pauli operators are

$$n_i = c_i^\dagger c_i = \frac{1 - Z_i}{2}, \tag{75}$$

$$c_i^\dagger c_j + c_j^\dagger c_i = \frac{1}{2}(X_i X_j + Y_i Y_j) Z_{i+1} \dots Z_{j-1}, \tag{76}$$

$$i(c_i^\dagger c_j - c_j^\dagger c_i) = \frac{1}{2}(Y_i X_j - X_i Y_j) Z_{i+1} \dots Z_{j-1}, \tag{77}$$

where we assume $j > i$. The implementation of the corresponding evolution operators for these pure fermion operators requires circuits with phase shift $T(\theta)$ [Eq. (72)] or z rotation

$$R_z(\theta) = \begin{bmatrix} e^{i\frac{\theta}{2}} & 0 \\ 0 & e^{-i\frac{\theta}{2}} \end{bmatrix} \tag{78}$$

gates [6,7].

The implementation of the fermion-boson interaction is similar. In the case of fermions coupling with the boson position operator X [Eqs. (19) and (21)] the only difference is the rotation angle θ, which is replaced by θx, where x is the eigenvalue of $\tilde{X}$ corresponding to the boson state $|x\rangle$. For example, in Fig. 7 we show the implementation of

$$e^{-i\theta c_i^\dagger c_i \tilde{X}_n}|i\rangle \otimes |x_n\rangle = (T(\theta x_n)|i\rangle) \otimes |x_n\rangle, \tag{79}$$

where $|i\rangle$ is the i fermion orbital and $|x_n\rangle$ is the state of the harmonic oscillator n.

The evolution of the term coupling the fermion hopping operator to the boson position operator can be written as

$$e^{-i\theta(c_i^\dagger c_j + c_j^\dagger c_j)\tilde{X}_n} \approx \mathcal{Y}_i^\dagger \mathcal{Y}_j^\dagger e^{-i\theta Z_i Z_{i+1} \dots Z_j \tilde{X}_n} \mathcal{Y}_j \mathcal{Y}_i \times H_i H_j e^{-i\theta Z_i Z_{i+1} \dots Z_j \tilde{X}_n} H_j H_i. \tag{80}$$

Since H (Hadamard) and $\mathcal{Y}$ [$\mathcal{Y} = R_x(\frac{\pi}{2})$] operators satisfy $HXH = Z$ and $\mathcal{Y}^\dagger Y \mathcal{Y} = Z$, they are employed to rotate the Pauli X and Y operators, respectively [see Eq. (76)], to the Z operator. The circuit is shown in Fig. 8. It is similar to the circuit shown in Fig. 9 of Ref. [7] or Table A1 of Ref. [6] for $e^{-i\theta(c_i^\dagger c_j + c_j^\dagger c_i)}$. The difference is that $R_z(\theta)$ is replaced by $R_z(\theta x_n)$. The circuit for $R_z(\theta x_n)$ is similar to the one shown in Fig. 7, the only difference being that T (the phase shift gate) is replaced by R_z (the z-rotation gate).

The evolution of the term coupling the fermion current operator [see Eq. (76)] to the boson position operator is

$$e^{-i\theta i(c_i^\dagger c_j - c_j^\dagger c_j)\tilde{X}_n} \approx H_i \mathcal{Y}_j^\dagger e^{i\theta Z_i Z_{i+1} \dots Z_j \tilde{X}_n} \mathcal{Y}_j H_i \times \mathcal{Y}_i^\dagger H_j e^{-i\theta Z_i Z_{i+1} \dots Z_j \tilde{X}_n} H_j \mathcal{Y}_i. \tag{81}$$

The circuit is analogous the one shown in Fig. 8, but the order of the single-qubit operators acting on the i fermion orbital is $\mathcal{Y}\mathcal{Y}^\dagger HH$ instead of $HH\mathcal{Y}\mathcal{Y}^\dagger$ (on the j fermion qubit the order

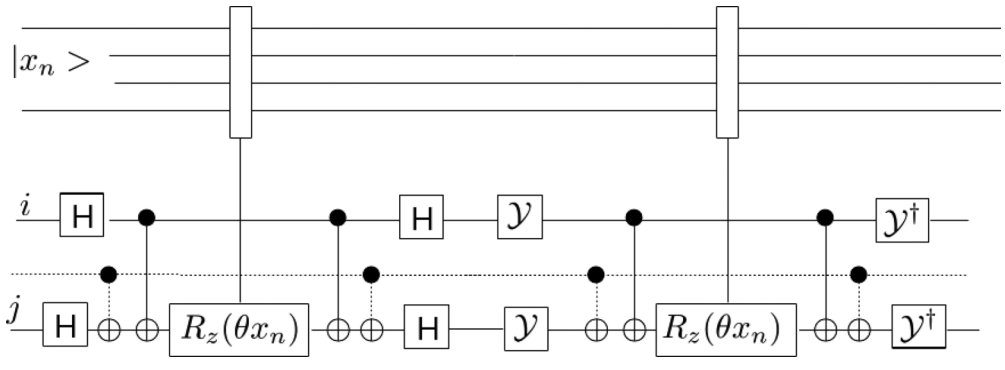

FIG. 8. The circuit implementing $e^{-i\theta(c_i^\dagger c_j + c_j^\dagger c_i)\tilde{X}_n}$ is similar to the circuit for the fermion hopping term (see Fig. 9 of Ref. [7] or Table A1 of Ref. [6]). The angle of the z-rotation gates is θx_n.

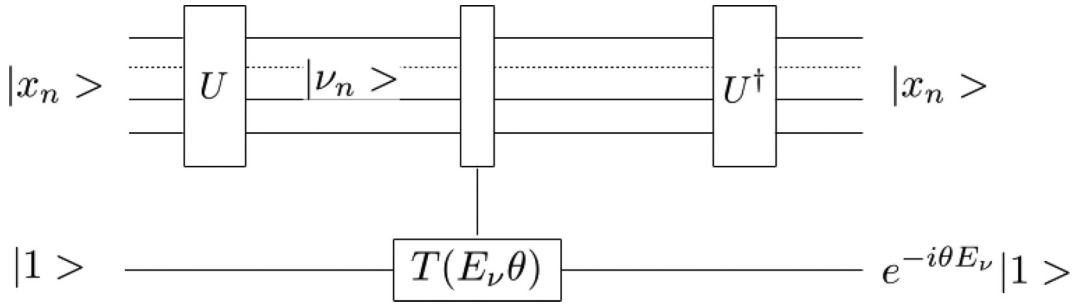

FIG. 9. The circuit implementing $e^{-i\theta H_{xp}}$. The unitary operator U transforms the position vectors $|x\rangle$ into the eigenvectors $|\nu\rangle$ of H_{xp}. For every state $|\nu\rangle$ a phase shift with the angle $E_\nu\theta$ is applied to an ancilla qubit prepared in state $|1\rangle$.

remains the same, $HH\mathcal{Y}\mathcal{Y}^\dagger$). The other difference is that the rotation angle corresponding to the second R_z gate changes sign, i.e., it is $-\theta x_n$ instead of θx_n.

For the cases when the fermions couple to the boson momentum operator P as in Eqs. (20) and (22), the circuits are analogous to the ones corresponding to Eqs. (19) and (21), respectively. The main difference is that the rotation angle acting on the fermion qubits is proportional to θp instead of θx. The value p is the eigenvalue of $\tilde{P}$ corresponding to the boson state $|p\rangle$ in the momentum representation. The state $|p\rangle$ is obtained by applying QFT to $|x\rangle$ at the beginning of the circuit. An inverse QFT transformation should be applied at the end of the circuit from $|p\rangle$ to $|x\rangle$ to restore the position representation.

The nonlocality of the Jordan-Wigner mapping increases the circuit depth for the fermionic terms in the Hamiltonian [4,6,7]. In the case when the fermion-boson coupling involves the fermion hopping operator, the additional contribution to the circuit depth of the Jordan-Wigner strings associated with the fermion-boson interaction can be avoided by combining the implementation of the fermion and fermion-boson terms. For example, for a coupling type characteristic of electron-phonon systems such as in Eq. (19), one can implement

$$e^{-i(c_i^\dagger c_j + c_i^\dagger c_j)(\theta_0 + \sum_m \theta_m \tilde{X}_m)}, \tag{82}$$

which reduces to the circuit shown in Fig. 8 with $R_z(\theta_0 + \sum_m \theta_m x_m)$ gates replacing the $R_z(\theta x_n)$ ones. In this case, the contribution to the circuit depth for long-range fermion-boson interactions is $O(N)$.

E. Squeezing and boson-boson interaction Hamiltonian

As discussed in Sec. II B 1, the implementation of the squeezing Hamiltonian (12) and the boson-boson interaction Hamiltonian (13) reduces to the implementation of terms of type A_nA_m, $A_nA_mA_r$, and $A_nA_mA_rA_s$, where A_n is either the X_n or the P_n operator of the harmonic oscillator n.

The implementation of terms A_nA_m $(n \neq m)$ present in the squeezing Hamiltonian (17) was described in Sec. IV B. The implementation of the interaction terms which do not contain self-interacting XP products such as $X_n^v P_n^u$ where $v, u > 0$ integers is a straightforward generalization. For example, the corresponding circuit for $A_nA_mA_rA_s$ consists of phase shift, controlled phase shift, double-controlled phase shift, and triple-controlled phase shift gates applied on the qubits of the boson registers n, m, r, and s. The angles of the phase shift gates are determined by writing $a_na_ma_ra_s$ as a sum with binary coefficients, where a_n is the eigenvalue of the operator A_n corresponding to the state of the boson register n. For $A_n \equiv P_n$, the circuit starts with a QFT and ends with an inverse QFT on the boson register n.

The implementation of the terms written as products of the X and P operators, such as $H_{xp} = X_n^u P_n^v + P_n^v X_n^u$, is more difficult. Such terms appear in the squeezing Hamiltonian (17). The problem is due to the fact that neither $|x\rangle$ nor $|p\rangle$ are eigenvectors of H_{xp}. A general approach for calculating $e^{-i\theta H_{xp}}$ is the following. First, the eigenproblem of the Hamiltonian $H_{xp} = \tilde{X}^u\tilde{P}^v + \tilde{P}^v\tilde{X}^u$ acting on the $N_x = 2^{n_x}$ size space is solved numerically on a classical computer,

$$H_{xp}|\nu\rangle = E_\nu|\nu\rangle, \tag{83}$$

$$|\nu\rangle = \sum_{x=0}^{N_x-1} U_{\nu x}|x\rangle. \tag{84}$$

Second, since U in Eq. (84) is unitary, a circuit for it can be designed [43,44]. The number of gates required for U scales as 4^{n_x}. The circuit for the evolution of H_{xp} is shown in Fig. 9. It starts with the transformation U applied to the boson register, which changes the position vectors to the H_{xp}'s eigenvectors, $|x\rangle \xrightarrow{U} |\nu\rangle$. The next step is a gate yielding a phase factor $\exp(-i\theta E_\nu)$. Since E_ν is calculated numerically a direct way to implement this is using 2^{n_x} multi(n_x)-controlled CNOT gates acting on an ancilla qubit [45]. Because n_x-controlled gates scale as $O(n_x^2)$ [43], the total number of gates required for the phase shift operation scales as $n_x^2 2^{n_x}$. The circuit ends with the transformation $U^\dagger$ applied to the boson register $|\nu\rangle \xrightarrow{U^\dagger} |x\rangle$.

Note that the circuits for the self-interacting boson terms containing XP products scale exponentially with n_x. All the other circuits for the fermion-boson model scale polynomial with n_x. Nevertheless, remember that a n_x exponential scaling is a polynomial scaling with the boson cutoff number (since $N_{ph} \propto N_x$). Moreover, the overall scaling of the full algorithm with the system size N is not changed (i.e., remains polynomial) since n_x is constant (does not depend on N).

F. Resource scaling

Fermion-boson interacting systems are represented on a number of qubits which scale linearly with the system size. Aside from the fermion-reserved qubits which scale linearly with the system size, the number of additional qubits required to represent the boson space is $O(Nn_x)$, where N is the system size and n_x is the number of qubits necessary to map the low-energy Hilbert space of a single harmonic oscillator. Equation (48) implies that n_x scales as

$$n_x = \log_2 N_x = O(\log_2[\ln(\epsilon^{-1}) + 0.765 N_{ph}(\epsilon^{-1})]), \quad (85)$$

where ϵ is the precision and N_{ph} is the maximum boson cutoff number. The boson cutoff number N_{ph} is dependent on the target precision ϵ. From Eq. (85) one can infer that, as long as N_{ph} increases with increasing $1/\epsilon$ slower than $[\ln(\epsilon^{-1})]^u$, with $u > 0$ being an arbitrary constant, then

$$n_x = O(\log_2[\ln(\epsilon^{-1})]). \quad (86)$$

That is the case for problems discussed in Sec. III D where the boson states evolve under the action of an effective forced harmonic oscillator Hamiltonian; see Eq. (60). Equations (61), (62), and (85) also imply that n_x scales as

$$n_x = O(\log_2(|\zeta_{\max}|^2)), \quad (87)$$

$$n_x = O(\log_2(N_E)), \quad (88)$$

where, as discussed in Sec. III D, $|\zeta_{\max}|^2$ and N_E are the effective coupling strength and the size of the low-energy space under consideration, respectively. For many problems, such as electron-phonon models, we found that a small number of qubits, $n_x \approx 6 \sim 7$, is enough to accurately ($\epsilon < 10^{-4}$) accommodate even the strong coupling regime.

Fermion-boson interacting systems can be simulated in polynomial time. The estimation of the number of gates in the following analysis is for one Trotter step. The number of gates and the circuit depth for simulating a single harmonic oscillator is $O(n_x^2)$. An m-body type boson-boson interaction (m-leg vertex interaction) term requires $O(n_x^m)$ gates. Boson self-interaction terms of type XP (see Sec. IV E) require $O(4^{n_x})$ gates.

When the fermion-boson interaction and the boson-boson coupling have finite range, as is the case for many physical models of interest in condensed matter physics, the bosons introduce an $O(N)$ contribution to the total number of gates and a constant contribution to the circuit depth. For general long-range fermion-boson interaction the number of gates and circuit depth scale as $O(N^2)$. When the bosons couple to the fermion hopping, as it is the case for electron-phonon models, the additional depth scales as $O(N)$. For long-range m-leg vertex boson-boson interactions, the number of gates and circuit depth scale as $O(N^m)$.

G. Input state preparation

The QPE algorithm requires an input state which has a large overlap with the ground state of the system. The preparation of this state can be done using the adiabatic method [40]. We start with a Hamiltonian $H_0 = H_f + H_{h0}$, where H_{h0} is the sum of the uncoupled harmonic oscillators, and then slowly turn on the fermion-boson and boson-boson couplings. The ground state of H_0 is $|f_0\rangle \otimes |\Phi_0\rangle$, where $|f_0\rangle$ is the fermion Hamiltonian ground state. Its preparation, while nontrivial, is addressed in the literature [3,6,7,46]. The state $|\Phi_0\rangle = \prod_n \otimes |\tilde{\phi}_{0n}\rangle$ is the ground state of H_{h0} and is a direct product of the harmonic oscillators ground-state functions $|\tilde{\phi}_{0n}\rangle$, where n is the harmonic oscillator site label. The state $|\tilde{\phi}_{0n}\rangle$ is the zeroth-order HG function on the 2^{n_x} grid, i.e., $|\tilde{\phi}_{0n}\rangle = |\chi_0\rangle$ [see Eq. (34)]. The preparation of $|\Phi_0\rangle$ therefore requires N discrete Gaussian states in parallel, each state prepared on a register of n_x qubits.

Methods to prepare Gaussian states are discussed in Refs. [47,48]. These methods require quantum computation of integrals, as well as arcosine and square-root functions, with high precision, which might not be feasible on near-future computers with limited resources.

When n_x is of the order of a few qubits, as it is for most electron-phonon problems of interest, including our polaron example (Sec. V, below), different methods can be employed to prepare a Gaussian on a grid. One choice is the brute force approach. The method is similar to the one described in Ref. [48], but the rotation angles for each configuration are precomputed and implemented using $(n_x - 1)$-controlled qubits. Since there are 2^{n_x} configurations and a $(n_x - 1)$-controlled qubits rotation scales as $O(n_x^2)$ [43], the corresponding circuit depth is $O(n_x^2 2^{n_x})$. The circuit depth is independent of the system size.

Another possibility for small-register Gaussian state preparation which is better suited for near-future quantum computers with limited coherence time is a variational method. We find heuristically that Gaussian states can be obtained with high fidelity by applying a N_S-step unitary operator on the state $|x = 0\rangle$,

$$|\phi_v\rangle = \prod_{s=1}^{N_S} U^s(\boldsymbol{\theta}^s, \boldsymbol{\rho}^s)|x = 0\rangle, \quad (89)$$

where

$$U^s(\boldsymbol{\theta}^s, \boldsymbol{\rho}^s) = \prod_{i=0}^{n_x-1} (e^{-i\theta^s_{yi} Y_i} e^{-i\theta^s_{xi} X_i} e^{-i\theta^s_{zi} Z_i}) \times e^{-i\rho^s_x \tilde{X}^2} e^{-i\rho^s_p \tilde{P}^2}. \quad (90)$$

The operators $e^{-i\rho^s_p \tilde{P}^2}$ and $e^{-i\rho^s_x \tilde{X}^2}$ require circuits with depth proportional to n_x, as described in Sec. IV B. The single-qubit x, y, and z rotations, $e^{-i\theta^s_x X}$, $e^{-i\theta^s_y Y}$, and $e^{-i\theta^s_z Z}$, respectively, increase the circuit depth by 3 gates per step since they can be implemented in parallel. The varational parameters $\boldsymbol{\theta}^s = \{\theta^s_{xi}, \theta^s_{yi}, \theta^s_{zi}\}_{i=\overline{0,n_x-1}}$ and $\boldsymbol{\rho}^s = \{\rho^s_x, \rho^s_p\}$ are determined by maximizing the fidelity $|\langle\phi_v|\chi_0\rangle|^2$. The circuit depth for the variational preparation of a Gaussian state is proportional to the number of steps N_S.

For large systems it is necessary to prepare local Gaussian states with high precision $\approx N^{-1}$. This can be understood from the following argument. If for a single harmonic oscillator the overlap between the prepared function and the Gaussian is $|\langle\phi|\chi_0\rangle|^2 = 1 - \epsilon$, then the overlap of the wave function corresponding the N harmonic oscillators with $|\Phi_0\rangle$ is $|\langle\phi|\chi_0\rangle|^{2N} \approx 1 - N\epsilon$.

By employing Eq. (89) and the simultaneous perturbation stochastic approximation method [49] for the optimization of $\{\boldsymbol{\theta}^s, \boldsymbol{\rho}^s\}$ parameters, we find that Gaussian states on $n_x = 6,\ 7,$ and 8 qubit registers can be prepared with fidelity larger than 0.988, 0.983, and 0.981, respectively, in $N_S = 3$ steps, and fidelity larger than 0.999, 0.998, and 0.996, respectively, in $N_S = 6$ steps. The fidelity values corresponding to $N_S = 3$ ($N_S = 6$) are large enough for quantum computations of systems with $N \sim 100$ ($N \sim 1000$) boson sites.

A systematic investigation of the variational approach to Gaussian states preparation, including an analysis of fidelity dependence on n_x and N_S, remains to be addressed in a future study. Here, we simply show that there is a practical and efficient way to prepare Gaussian states on small-register qubits.

H. Measurements

Measurement methods for quantum algorithms simulating many-particle systems, including local and time-dependent correlation functions, have been described previously; see for example Refs. [4,7]. These methods can be applied to our fermion-boson model as well. For example, to calculate the phonon distribution number in the Holstein polaron (in Sec. V) we use QPE for the unitary operator obtained by exponentiating the boson number.

V. BENCHMARKING THE HOLSTEIN POLARON ON A QUANTUM SIMULATOR

The bound state of an electron and its surrounding phonons is called a polaron. The polaron problem has been addressed extensively in the literature. In the Holstein model [25] the phonons are described as a set of independent oscillators located at every site. The electron density at a particular site couples to the displacement of the harmonic oscillator located at the same site:

$$H = -t\sum_{ij}(c_i^\dagger c_j + c_j^\dagger c_i) + g\sum_i c_i^\dagger c_i X_i + \sum_i \frac{P_i^2}{2} + \frac{1}{2}\omega^2 X_i^2. \tag{91}$$

The two-site polaron problem is small enough to be solved exactly using the diagonalization method on a conventional computer. The size of the local phonon Hilbert space is truncated by a cutoff large enough to reach convergence, i.e., results no longer change with increasing cutoff. In our case a cutoff of $N_{ph} \approx 45$ phonons per site is sufficient for convergence.

In order to check the validity of our algorithm we ran a QPE code for the Holstein polaron on a two-site lattice using an Atos Quantum Learning Machine simulator. A comparison between exact diagonalization and our quantum algorithm is shown in Fig. 10. The figure shows the energy of the polaron as a function of the dimensionless coupling constant $\alpha = g^2/2\omega^2 t$, defined as a ratio of lattice deformation energy $g^2/2\omega^2$ to electron kinetic energy t. The agreement is very good, with a difference of $O(10^{-4})$ due mainly to the use of the Trotter approximation. A register of size $n_x = 6$ qubits

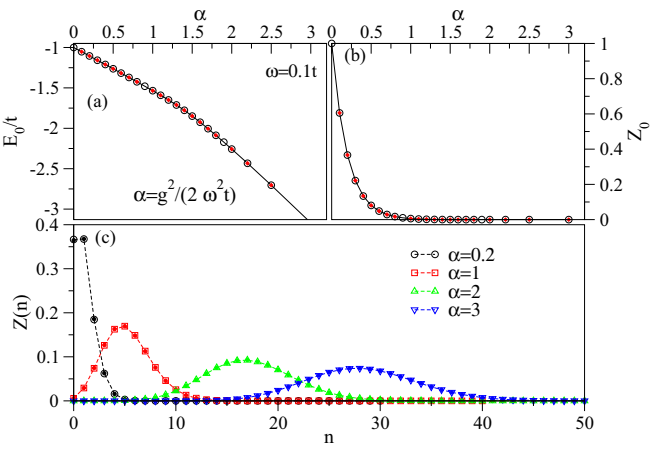

FIG. 10. The energy (a) and quasiparticle weight (b) for the two-site Holstein polaron versus electron-phonon coupling strength. (c) The phonon-number distribution in the polaron state for different values of the coupling strength. The open symbols are computed using the exact diagonalization technique while the full small circles are computed using the QPE algorithm on a quantum simulator. The state of each harmonic oscillator was stored in a $n_x = 6$ qubit register.

for each harmonic oscillator is large enough to accurately describe the physics even in the strong coupling regime.

One can see that even this simple two-site model captures some essential features of more realistic polarons. The transition from a light polaron to a heavy polaron as a function of the coupling strength is smooth, similar to what is seen in 1D polaron models [50].

The polaron state can be written as

$$|\Phi\rangle = \sum_{n=0}\sum_r a_{nr}|n, r\rangle, \tag{92}$$

where $\{|n, r\rangle\}_r$ are normalized vectors spanning the sector of the Hilbert space with one electron and n phonons. The phonon distribution in the polaron state is defined as $Z(n) = \sum_r |a_{nr}|^2$ and can be determined by applying the QPE algorithm for the phonon evolution Hamiltonian $H_p = \sum_i \frac{P_i^2}{2} + \frac{1}{2}\omega^2 X_i^2$. Since $|\Phi\rangle$ is not an eigenstate of H_p, the energy $E_n = \omega(n + \frac{1}{2})$ is measured with the probability $Z(n)$.

The quasiparticle weight $Z(0)$ as a function of the coupling strength is shown in Fig. 10(b). This quantity represents the amount of the free electron in the polaron state and gives the quasiparticle weight measured in the photoemission experiments. In Fig. 10(c), $Z(n)$ is shown for several values of the coupling strength corresponding to weak, intermediate, and strong coupling regimes. The exact diagonalization and the QPE results agree well with each other.

Note that by employing a rotation of the oscillator coordinates such as $X_1' = (X_1 + X_2)/\sqrt{2}$ and $X_2' = (X_1 - X_2)/\sqrt{2}$, the two-site Holstein polaron problem can be reduced to a single harmonic oscillator interacting with a two-level system. However, we have not used this transformation to reduce the degrees of freedom of the problem since our purpose is benchmarking the algorithm.

VI. DISCUSSION

Our algorithm assumes that, within a controlled approximation, each harmonic oscillator space can be truncated to a finite size. Since at every Trotter step the state of each harmonic oscillator is a linear combination of displaced low-energy states (see Sec. III D), one expects that for electron-phonon models the number of phonons in a localized basis can be truncated with exponential accuracy as long as the system is stable.

Nevertheless, there are many physical system characterized by boson states with large occupancy where the implementation of our algorithm might be questionable. In many cases, a convenient choice of the boson basis might solve the truncation problem. For example, it is evident that trying to employ the algorithm for a boson system having the zero-momentum state macroscopically occupied, as in case of Bose-Einstein condensates, does not work if the harmonic oscillator labels represent momentum states. However, the truncation of the boson space might be feasible in the localized basis since the number of bosons per site is small. In Appendix C we show that the local occupation distribution of a zero-momentum macroscopically occupied state goes quickly to zero with increasing boson number.

Phase-squeezed states, commonly encountered in quantum optics, are another example of states with large boson-number distributions. Nevertheless, the scaling equation for the boson register size derived for electron-phonon problems, Eq. (86), is also valid in this case. This can be inferred by noticing that the photon-number distribution goes to zero exponentially quickly with increasing photon number. As shown in Ref. [34], the probability P_n to have n photons in a squeezed state is proportional to $\frac{C^n}{n!}$, where C is independent of n. Using the Stirling formula $n! \approx \sqrt{2\pi n}(n/e)^n$, one can see that once $n > eC$, P_n goes to zero faster than exponentially with increasing n. However, C can be large when the squeezing parameter is large. In that case, the squeezed state contains a large number of photons and, consequently, its representation requires a large qubit register.

The possibility of implementing a simple and efficient displacement operator is the main merit of the boson-space representation in our algorithm. While the truncation of the boson space can be done more naturally in the boson-number basis, we are not aware of the existence of any efficient algorithm for the evolution of the forced harmonic oscillator in this basis.

Our work points to further directions of exploration. Although we focus on electron-phonon interactions, our algorithm may be viewed as a first step towards simulating other interesting systems with these ingredients, QED and QCD among them. For example, the Hamiltonian representation of lattice gauge theories [51] possesses some structural similarities to the electron-phonon system. Pure gauge lattice Hamiltonians have been mapped onto quantum simulation schemes in [52,53] using different discretization schemes. It is interesting to consider applying this truncation of the Hilbert space to more fundamental quantum field theories in order to understand the relationship between the cutoff in the number of bosons and regularization approaches.

VII. CONCLUSIONS

We introduce a quantum algorithm for nonrelativistic fermion-boson interacting systems which extends the existing quantum fermion algorithms to include bosons. The algorithm can address boson-boson interactions as well. The bosons are represented as a set of harmonic oscillators. Each harmonic oscillator space is reduced to a finite-sized Hilbert space $\tilde{\mathcal{H}}$. We define operators $\tilde{X}$ and $\tilde{P}$ on $\tilde{\mathcal{H}}$ and show that, in the low-energy subspace, the algebra generated by $\{\tilde{X}, \tilde{P}\}$ is, up to an exponentially small error, isomorphic with the algebra generated by $\{X, P\}$. The exponentially good representation is a consequence of the properties of the Hermite-Gaussian functions. Since they fall exponentially fast to zero at large argument the Nyquist-Shannon theorem can be applied. The Nyquist-Shannon theorem ensures both the truncation of the HG functions to a finite set of points and the fact that the discrete Fourier transform is the same as the continuous Fourier transform at the grid points. The equivalence between the discrete and continuous Fourier transforms makes possible the definition of the operators $\tilde{X}$ and $\tilde{P}$ obeying the canonical commutation relation in the low-energy subspace. The size of the low-energy subspace is determined by the maximum order of the HG functions whose width is covered by the grid size and it is equivalent to a cutoff in boson number N_{ph}. The minimum size of the finite space $\tilde{\mathcal{H}}$ required to accurately represent N_{ph} bosons increases approximately linearly with N_{ph}.

Our algorithm maps all harmonic oscillator spaces $\tilde{\mathcal{H}}$ on the qubit space and simulates the evolution operator of the fermion-boson Hamiltonian. The algorithm utilizes Trotter decomposition in small evolution steps. We present circuits for the implementation of small evolution steps corresponding to free boson, boson-boson interaction, and fermion-boson interaction terms in the Hamiltonian.

The number of qubits necessary to store the bosons scales logarithmically with the maximum boson-number cutoff. For electron-phonon systems we find that a small number of qubits, $n_x \approx 6, 7$ per harmonic oscillator, is large enough for the simulation of weak, intermediate, and strong coupling regimes of most problems of physical interest. The number of additional qubits required to add the boson space to a fermion system is $O(N)$ where N is proportional to the system size. For finite-range fermion-boson and boson-boson interactions, the bosons introduce a $O(N)$ contribution to the total number of gates and a constant contribution to the circuit depth. For general long-range fermion-boson interactions, the number of gates and circuit depth scale as $O(N^2)$. When the bosons couple to the fermion hopping, as is the case for electron-phonon models, the additional depth scales as $O(N)$. For long-range m-leg vertex boson-boson interactions, the number of gates and circuit depth scale as $O(N^m)$.

We benchmarked our algorithm on an Atos QLM simulator for a two-site Holstein polaron, employing the QPE method. The polaron energy and phonon distribution are in excellent agreement with the ones calculated by exact diagonalization.

ACKNOWLEDGMENTS

We thank A. Li, E. Stern, P. Fox, and K. Howe for discussions. This manuscript has been authored by Fermi Research

Alliance, LLC, under Contract No. DE-AC02-07CH11359 with the US Department of Energy, Office of Science, Office of High Energy Physics. We gratefully acknowledge the computing resources provided and operated by the Joint Laboratory for System Evaluation (JLSE) at Argonne National Laboratory. We would like to thank Atos for the use of their 38-Qubit Quantum Learning Machine (QLM) and support of their universal programming language AQASM.

APPENDIX A: HERMITE-GAUSS FUNCTIONS ON A DISCRETE GRID

In this appendix, we will show that, after the truncation to a discrete grid, the discrete Fourier transform preserves the correspondence between the direct and the Fourier-transformed space of the Hermite-Gauss functions with exponential precision. This result is a consequence of the Nyquist-Shannon sampling theorem [22] and the exponential falloff of the Hermite-Gauss (HG) functions at large argument.

The HG functions $\phi_n(x)$ [Eq. (26)] and their Fourier transforms $\hat{\phi}_n(p)$ [Eq. (27)] fall exponentially fast to zero for large argument. The width of the HG functions increases monotonically with increasing n. Therefore, for any positive integer cutoff N_{ph}, a half-width L can be chosen such that for all $n < N_{ph}$, $|\hat{\phi}_n(p)| < \epsilon$ for $|p| > L$ and $|\phi_n(x)| < \epsilon$ for $|x| > L$, where $\epsilon \propto e^{-\frac{L^2}{2}}$ is exponentially small.

Let us define a periodic function $\overline{\phi}_n(p) = \phi_n(p)$ for $p \in [-L, L]$ with the property $\overline{\phi}_n(p) = \overline{\phi}_n(p + 2L)$ and choose L large enough such that

$$\phi_n(p) = \overline{\phi}_n(p) R\Big(\frac{p}{2L}\Big) + O(\epsilon), \tag{A1}$$

where $R(t)$ is the rectangular function defined as

$$R(t) = \begin{cases} 1, & |t| \leqslant \frac{1}{2} \\ 0, & |t| > \frac{1}{2}. \end{cases} \tag{A2}$$

Since the function $\phi_n(x)$ is the Fourier transform $\phi_n(p)$, according to Eq. (A1) it can be written as a convolution of $\overline{\phi}_n(x)$ and $v(x)$:

$$\begin{aligned} \phi_n(x) &= \int \overline{\phi}_n(y) v(x - y) dy + O(\epsilon) \\ &= \sum_{i=-\infty}^{\infty} \overline{\phi}_n(x_i) v(x - x_i) + O(\epsilon). \end{aligned} \tag{A3}$$

In Eq. (A3)

$$\begin{aligned} \overline{\phi}_n(x_i) &= \frac{1}{2L} \int_{-L}^{L} \overline{\phi}_n(p) e^{ipx_i} dp \\ &= \frac{1}{2L} \phi_n(x_i) + O(\epsilon) \end{aligned} \tag{A4}$$

is the Fourier transform of the periodic function $\overline{\phi}_n(p)$ defined for the discrete set of points $\{x_i = i\Delta\}_{i \in \mathbb{Z}}$, where $\Delta = \frac{\pi}{L}$. The function $v(x)$ is the Fourier transform of the rectangular function $R(\frac{p}{2L})$:

$$v(x) = \int R\Big(\frac{p}{2L}\Big) e^{ipx} dp = \int_{-L}^{L} e^{ipx} dp = 2\frac{\sin Lx}{x}. \tag{A5}$$

From Eqs. (A3), (A4), and (A5) one can write

$$\phi_n(x) = \sum_{i=-\infty}^{\infty} \phi_n(x_i) u_i(x) + O(\epsilon), \tag{A6}$$

with $u_i(x) = \frac{1}{2L} v(x - x_i)$.

In fact, if the exponentially small term $O(\epsilon)$ is neglected, Eq. (A6) is the well-known Nyquist-Shannon sampling theorem [22] which states that a band-limited function can be sampled without loss of information at points $x_i = i\frac{\pi}{L}$, where L is the band half-width. Note that $u_i(x) = \mathrm{sinc}(\frac{x - x_i}{\Delta})$ where $\mathrm{sinc}(x) = \frac{\sin(\pi x)}{\pi x}$ is the normalized sinc function, which is familiar in signal processing.

Since $\phi_n(x)$ is also exponentially small for $|x| > L$, the summation over i in Eq. (A6) can be truncated to the interval $[-L, L]$. The minimum number of points N_x necessary to sample the interval $[-L, L]$ should satisfy the equation $N_x \Delta = 2L$. Since $\Delta = \frac{\pi}{L}$, it follows that $2L = \sqrt{2\pi N_x}$ and $\Delta = \sqrt{\frac{2\pi}{N_x}}$.

The functions $u_i(x)$ appearing in Eq. (A6) form an orthonormal set

$$\int u_i(x) u_j(x) dx = 2\pi \int \hat{u}_i^*(p) \hat{u}_j(p) dp = \Delta \delta_{ij}, \tag{A7}$$

as can be easily checked by noticing that

$$\hat{u}_i(p) = \frac{1}{2\pi} \int u_i(x) e^{-ipx} dx = \frac{1}{2L} e^{-ipx_i} R\Big(\frac{p}{2L}\Big). \tag{A8}$$

Equations (A6) and (A7), together with the orthogonality property of the HG functions, imply

$$\begin{aligned} \delta_{nm} &= \int \phi_n(x) \phi_m(x) dx \\ &= \Delta \sum_{i=-\frac{N_x}{2}}^{\frac{N_x}{2}-1} \phi_n(x_i) \phi_m(x_i), \end{aligned} \tag{A9}$$

where we neglect writing the exponentially small term $O(\epsilon)$. Consequently, the N_x size vectors

$$\chi_n(x_i) = \sqrt{\Delta} \phi_n(x_i) \tag{A10}$$

form an orthonormal set. Note that this is not a complete set since Eq. (A9) is valid only for $n, m < N_{ph} < N_x$. The properties of the HG functions require $N_{ph} < N_x$, as implied by Eq. (33).

The Fourier transform of the HG functions can be written as

$$\begin{aligned} \hat{\phi}_n(p) &= \sum_{i=-\frac{N_x}{2}}^{\frac{N_x}{2}-1} \phi_n(x_i) \hat{u}_i(p) \\ &= \frac{1}{2L} \sum_{i=-\frac{N_x}{2}}^{\frac{N_x}{2}-1} \phi_n(x_i) e^{-ipx_i} R\Big(\frac{p}{2L}\Big). \end{aligned} \tag{A11}$$

Since $R(\frac{p}{2L}) = 1$ for $p \in [-L, L]$, up to an exponentially small error one can write

$$\hat{\phi}_n(p_m) = \frac{1}{2L} \sum_{i=-\frac{N_x}{2}}^{\frac{N_x}{2}-1} \phi_n(x_i) e^{-ip_m x_i}, \tag{A12}$$

where $p_m = m\Delta$ with $m = \overline{-N_x/2, N_x/2-1}$. This implies

$$\hat{\chi}_n(p_m) = \sqrt{2\pi\Delta}\hat{\phi}_n(p_m), \tag{A13}$$

where

$$\hat{\chi}_n(p_m) = \frac{1}{\sqrt{N_x}} \sum_{i=-\frac{N_x}{2}}^{\frac{N_x}{2}-1} \chi_n(x_i) e^{-ip_m x_i} \tag{A14}$$

is the discrete Fourier transform of the finite-size vector $\chi_n(x_i)$ defined in Eq. (A10). Equation (A13) shows that, when restricted to the grid points $\{x_i\} \longleftrightarrow \{p_m\}$, the discrete Fourier transform can replace the continuous Fourier transform of the HG functions with $n < N_{ph}$ with exponentially small error.

APPENDIX B: COHERENT STATES, DISPLACEMENT OPERATOR, AND THE FORCED HARMONIC OSCILLATOR

We list here some properties of boson coherent states and the forced harmonic oscillator relevant for the boson-number cutoff discussion presented in Sec. III D. The derivation of these results can be found in Refs. [34,37,54,55].

The displacement operator is defined as

$$D(z) = e^{zb^\dagger - z^* b}, \tag{B1}$$

where z is a complex number. The displacement operator has the following properties:

$$D^\dagger(z) b D(z) = b + z, \tag{B2}$$

$$D^\dagger(z) b^\dagger D(z) = b^\dagger + z^*, \tag{B3}$$

$$D(z_1)D(z_2) = e^{\frac{z_1 z_2^* - z_1^* z_2}{2}} D(z_1 + z_2). \tag{B4}$$

When applied to the vacuum, $D(z)$ creates the coherent state

$$|z\rangle \equiv D(z)|0\rangle = e^{-\frac{|z|^2}{2}} \sum_{n=0}^{\infty} \frac{z^n}{\sqrt{n!}} |\phi_n\rangle. \tag{B5}$$

The coherent states are eigenstates of the annihilation operator and have the following properties:

$$b|z\rangle = z|z\rangle, \tag{B6}$$

$$e^{-i\theta b^\dagger b}|z\rangle = |ze^{-i\theta}\rangle, \tag{B7}$$

$$\langle N\rangle = \langle b^\dagger b\rangle = |z|^2, \tag{B8}$$

$$\langle (\Delta N)^2\rangle = \langle (N - \langle N\rangle)^2\rangle = |z|^2. \tag{B9}$$

The boson occupation number of a coherent state is a Poisson distribution [see Eq. (B5)]

$$|\langle \phi_n | z\rangle|^2 = e^{-|z|^2} \frac{|z|^{2n}}{n!}. \tag{B10}$$

This distribution falls exponentially to zero with increasing n. The coherent states can be represented with accuracy ϵ on a finite-sized space truncated by a boson-number cutoff $N_c \gtrsim |z|^2 + |z|\sqrt{2\ln(\epsilon^{-1})}$.

The displacement matrix in the boson-number basis is

$$\langle \phi_m | D(z) | \phi_n\rangle = \sqrt{\frac{n!}{m!}} z^{m-n} e^{-|z|^2/2} L_n^{(m-n)}(|z|^2), \tag{B11}$$

where $L_n^{(m-n)}$ are the Laguerre polynomials [54,55]. The *displaced number states* are defined by applying the displacement operator to the number states,

$$|n, z\rangle = D(z)|\phi_n\rangle. \tag{B12}$$

A useful property of the displaced number states is

$$e^{-i\theta b^\dagger b}|n, z\rangle = e^{-in\theta}|n, ze^{-i\theta}\rangle, \tag{B13}$$

which can be obtained by expanding $|n, z\rangle$ in the $\{|\phi_m\rangle\}_m$ basis and employing Eq. (B11).

Using Eq. (B11) one can show that the boson-number distribution in the displaced number state $|n, z\rangle$ is Poissonian (see Ref. [55] for more details) with the mean and variance given by

$$\langle N\rangle = n + |z|^2, \tag{B14}$$

$$\langle (\Delta N)^2\rangle = (2n+1)|z|^2. \tag{B15}$$

The state $|n, z\rangle$ can be represented to accuracy ϵ on a finite-sized space truncated by a boson-number cutoff

$$N_c \gtrsim n + |z|^2 + |z|\sqrt{2(2n+1)\ln(\epsilon^{-1})}. \tag{B16}$$

The forced harmonic oscillator Hamiltonian

$$H = \frac{P^2}{2M} + \frac{1}{2}M\omega^2 + g(t)X + h(t)P \tag{B17}$$

is written in the second quantized form as

$$H = \omega\left(b^\dagger b + \tfrac{1}{2}\right) + f(t)b + f^*(t)b^\dagger, \tag{B18}$$

with $f(t) = [g(t)/\sqrt{M\omega} - ih(t)\sqrt{M\omega}]/\sqrt{2}$.

When f is constant, the forced harmonic oscillator is, up to a constant term $|f|^2/\omega$, the harmonic oscillator $H_0 = \omega(b^\dagger b + 1/2)$ displaced by f^*/ω:

$$D^\dagger\left(\frac{f^*}{\omega}\right) H_0 D\left(\frac{f^*}{\omega}\right) = H + \frac{|f|^2}{\omega}. \tag{B19}$$

Therefore, the eigenstates of H can be obtained from the eigenstates of H_0 by applying $D(f/\omega)$, i.e., are displaced number states $\{|n, f/\omega\rangle\}_n$ as defined by Eq. (B12).

One can show that the evolution operator of the Hamiltonian (B18) is [37]

$$U(t) = e^{i\beta(t)} D[\zeta(t)e^{-i\omega t}] e^{-iH_0 t} \tag{B20}$$

with

$$\beta(t) = \frac{i}{2}\int_0^t du \int_0^u ds f(u) f^*(s) e^{-i\omega(u-s)} \tag{B21}$$

$$-\frac{i}{2}\int_0^t du \int_0^u ds f^*(u) f(s) e^{i\omega(u-s)}, \tag{B22}$$

and

$$\zeta(t) = -i \int_0^t f^*(u) e^{i\omega u} du. \tag{B23}$$

Employing Eqs. (B4), (B13), and (B20), the evolution of a displaced number state is

$$U(t)|n, z\rangle = e^{i\gamma} e^{i(\beta - n\omega t)} |n, (\zeta + z)e^{-i\omega t}\rangle, \tag{B24}$$

where $\gamma = -i(\zeta z^* - \zeta^* z)/2$ is a real phase factor.

A state belonging to the finite-sized space determined by the N_E cutoff

$$|\phi\rangle = \sum_{n=0}^{N_E} c_n |\phi_n\rangle \tag{B25}$$

evolves under the forced harmonic oscillator action as

$$U(t)|\phi\rangle = \sum_{n=0}^{N_E} c_n e^{i(\beta - n\omega t)} |n, \zeta e^{-i\omega t}\rangle. \tag{B26}$$

Provided that $|\zeta(t)|_t < \zeta_{\max}$, the state $|\phi\rangle$ remains contained in the low-energy subspace defined by the new cutoff

$$N_{ph} = N_E + |\zeta_{\max}|^2 + |\zeta_{\max}| \sqrt{2(2N_E + 1)\ln(\epsilon^{-1})}, \tag{B27}$$

with ϵ accuracy.

APPENDIX C: LOCAL BOSON DISTRIBUTION OF A MACROSCOPICALLY OCCUPIED STATE WITH ZERO MOMENTUM

In this appendix we demonstrate that a zero-momentum state occupied by N bosons, where N is the system size, can be truncated to a finite number of bosons with exponential accuracy when $N \longrightarrow \infty$ if the truncation of the Hilbert space is done in the localized basis.

Let us consider N bosons on a lattice of size N. The boson creation operators in the momentum basis $\{\tilde{b}_k^\dagger\}$ are related to the boson creation operators in the localized basis $\{b_n^\dagger\}$ by

$$\tilde{b}_k^\dagger = \frac{1}{\sqrt{N}} \sum_{n=0}^{N-1} e^{ikr_n} b_n^\dagger. \tag{C1}$$

Next, we consider the state where all N particles have zero momentum

$$|\phi\rangle \equiv |N_{k=0}\rangle = \frac{1}{\sqrt{N!}} (\tilde{b}_0^\dagger)^N |0\rangle. \tag{C2}$$

Now, we ask what is the probability of having p bosons occupying a localized state labeled i. Expanding in a localized basis, the state $|\phi\rangle$ can be written as

$$|\phi\rangle = \sum_{p=0}^{N} w(p) |p_i\rangle |(N-p)_a\rangle, \tag{C3}$$

where

$$|p_i\rangle = \frac{1}{\sqrt{p!}} (b_i^\dagger)^p |0\rangle \tag{C4}$$

is the state with p bosons at site i, and $|(N-p)_a\rangle$ is a site with $N-p$ bosons anywhere else.

The calculation of the probability $|w(p)|^2$ for having p bosons on the site i is straightforward. If one defines the boson operator

$$a^\dagger = \frac{1}{\sqrt{N-1}} \sum_{\substack{n=0 \\ n \neq i}}^{N-1} b_n^\dagger, \tag{C5}$$

then the $k = 0$ creation operator can be written as

$$\tilde{b}_0^\dagger = \frac{1}{\sqrt{N}} \sum_{n=0}^{N-1} b_n^\dagger = \frac{1}{\sqrt{N}} (b_i^\dagger + \sqrt{N-1} a^\dagger). \tag{C6}$$

Introducing Eq. (C6) into Eq. (C2), one obtains

$$\begin{aligned} |\phi\rangle &= \frac{1}{\sqrt{N!}} \left(\frac{1}{\sqrt{N}}\right)^N \\ &\quad \times \sum_{p=0}^{N} \binom{N}{p} (\sqrt{N-1})^{N-p} (b_i^\dagger)^p (a^\dagger)^{N-p} |0\rangle \\ &= \left(\frac{\sqrt{N-1}}{\sqrt{N}}\right)^N \sum_{p=0}^{N} \sqrt{\binom{N}{p}} \frac{1}{\sqrt{N-1}^p} |p_i\rangle |(N-p)_a\rangle, \end{aligned} \tag{C7}$$

where

$$|(N-p)_a\rangle = \frac{1}{\sqrt{(N-p)!}} (a^\dagger)^{N-p} |0\rangle. \tag{C8}$$

It follows that

$$\begin{aligned} |w(p)|^2 &= \left(\frac{N-1}{N}\right)^N \frac{N(N-1)\ldots(N-p+1)}{p!(N-1)^p} \\ &< \frac{1}{p!} \left(\frac{N-1}{N}\right)^{N-1} \xrightarrow{N\longrightarrow\infty} \frac{1}{p!e}. \end{aligned} \tag{C9}$$

The occupation-number probability at a particular site falls as $1/p!$ with increasing the occupation number p. Therefore, the state $|\phi\rangle$ can be truncated with exponential accuracy on the Hilbert space obtained as a product of finite-sized local Hilbert spaces.

[1] D. S. Abrams and S. Lloyd, Simulation of Many-Body Fermi Systems on a Universal Quantum Computer, Phys. Rev. Lett. **79**, 2586 (1997).

[2] D. S. Abrams and S. Lloyd, Quantum Algorithm Providing Exponential Speed Increase for Finding Eigenvalues and Eigenvectors, Phys. Rev. Lett. **83**, 5162 (1999).

[3] G. Ortiz, J. E. Gubernatis, E. Knill, and R. Laflamme, Quantum algorithms for fermionic simulations, Phys. Rev. A **64**, 022319 (2001); Erratum: Quantum algorithms for fermionic simulations [Phys. Rev. A 64, 022319 (2001)], **65**, 029902(E) (2002).

[4] R. Somma, G. Ortiz, J. E. Gubernatis, E. Knill, and R. Laflamme, Simulating physical phenomena by quantum networks, Phys. Rev. A **65**, 042323 (2002).

[5] R. D. Somma, G. Ortiz, E. H. Knill, and J. Gubernatis, *Quantum Simulations of Physics Problems*, SPIE Proceedings Volume 5105, Quantum Information and Computation (SPIE, Bellingham, WA, 2003).

[6] J. D. Whitfield, J. Biamonte, and A. Aspuru-Guzik, Simulation of electronic structure Hamiltonians using quantum computers, Mol. Phys. **109**, (2011).

[7] D. Wecker, M. B. Hastings, N. Wiebe, B. K. Clark, C. Nayak, and M. Troyer, Solving strongly correlated electron models on a quantum computer, Phys. Rev. A **92**, 062318 (2015).

[8] A. Peruzzo, J. McClean, P. Shadbolt, M.-H. Yung, X.-Q. Zhou, P. J. Love, A. Aspuru-Guzik, and J. L. O'Brien, A Variational Eigenvalue Solver on a Photonic Quantum Processor, Nat. Commun. **5**, 4213 (2014).

[9] J. R. McClean *et al.*, The theory of variational hybrid quantum-classical algorithms, New J. Phys. **18**, 023023 (2016).

[10] S. B. Bravyi and A. Y. Kitaev, Fermionic Quantum Computation, Ann. Phys. **298**, 10 (2002).

[11] L. A. Wu and D. A. Lidar, Qubits as parafermions, J. Math. Phys. **43**, 4506 (2002).

[12] C. D. Batista and G. Ortiz, Algebraic approach to interacting quantum systems, Adv. Phys. **53**, 1 (2007).

[13] S. P. Jordan, K. S. M. Lee, and J. Preskill, Quantum Algorithms for Quantum Field Theories, Science **336**, 1130 (2012).

[14] J. Casanova, L. Lamata, I. L. Egusquiza, R. Gerritsma, C. F. Roos, J. J. Garcia-Ripoll, and E. Solano, Quantum Simulation of Quantum Field Theories in Trapped Ions, Phys. Rev. Lett. **107**, 260501 (2011).

[15] J. Casanova, A. Mezzacapo, L. Lamata, and E. Solano, Quantum Simulation of Interacting Fermion Lattice Models in Trapped Ions, Phys. Rev. Lett. **108**, 190502 (2012).

[16] A. Mezzacapo, J. Casanova, L. Lamata, and E. Solano, Digital Quantum Simulation of the Holstein Model in Trapped Ions, Phys. Rev. Lett. **109**, 200501 (2012).

[17] L. Lamata, A. Mezzacapo, J. Casanova, and E. Solano, Efficient quantum simulation of fermionic and bosonic models in trapped ions, EPJ Quantum Technol. **1**, 9 (2014).

[18] C. Clay Marston and G. G. Balint Kurti, The Fourier grid Hamiltonian method for bound state eigenvalues and eigenfunctions, J. Chem. Phys. **91**, 3571 (1989).

[19] J. C. Light, I. P. Hamilton, and J. V. Lill, Generalized discrete variable approximation in quantum mechanics, J. Chem. Phys. **82**, 1400 (1985).

[20] Robert G. Littlejohn and M. Cargo, A general framework for discrete variable representation basis sets, J. Chem. Phys. **116**, 8691 (2002).

[21] A. Bulgac and M. McNeil Forbes, Use of the discrete variable representation basis in nuclear physics, Phys. Rev. C **87**, 051301(R) (2013).

[22] C. E. Shannon, Communication in the presence of noise, Proc. Institute Radio Eng. **37**, 10 (1949).

[23] P. Jordan and E. Wigner, Über das Paulische Äquivalenzverbot, Z. Phys. A **47**, 631 (1928).

[24] L. Landau, Electron Motion in Crystal Lattices, Z. Phys. **3**, 664 (1933).

[25] T. Holstein, Studies of polaron motion: Part I. The molecular-crystal model, Ann. Phys. (NY) **8**, 325 (1959).

[26] A. Yu. Kitaev, Quantum measurements and the Abelian Stabilizer Problem, arXiv:quant-ph/9511026.

[27] R. Cleve, A. Ekert, C. Macchiavello, and M. Mosca, Quantum Algorithms Revisited, Proc. R. Soc. London A **454**, 339 (1998).

[28] A. Y. Kitaev, A. H. Shen, and M. N. Vyalyi, *Classical and Quantum Computation* (American Mathematical Society, Providence, RI, 2002), Vol. 47.

[29] M. A. Nielsen and I. L. Chuang, *Quantum Computation and Quantum Information* (Cambridge University Press, Cambridge, UK, 2010).

[30] A. Aspuru-Guzik, A. D. Dutoi, P. J. Love, and M. Head-Gordon, Simulated quantum computation of molecular energies, Science **309**, 1704 (2005).

[31] A. S. Alexandrov and J. T. Devreese, *Advances in Polaron Physics* (Springer, New York, 2010), Chap. 1.

[32] C. Kittel, *Quantum Theory of Solids*, 2nd revised ed. (Wiley, New York, 1987), Chap. 7.

[33] F. Giustino, Electron-phonon interactions from first principles, Rev. Mod. Phys. **89**, 015003 (2017).

[34] C. C. Gerry and Knight, *Introductory Quantum Optics* (Cambridge University Press, Cambridge, 2005), Chap. 7. See Eq. (7.81) for the photon-number distribution in squeezed states.

[35] S. Gradshteyn and I. M. Ryzhik, *Tables of Integrals, Series and Products* (Academic, New York, 1965), formula 7.376.

[36] $H_{n+1}(x) = 2xH_n(x) - 2nH_{n-1}(x)$. See *Handbook of Mathematical Functions with Formulas, Graphs, and Mathematical Tables*, edited by M. Abramowitz and I. A. Stegun, 9th printing (Dover, New York, 1972), Chap. 22.7.

[37] E. Merzbacher, *Quantum Mechanics*, 3rd ed. (Wiley, New York, 1998); Chapters 7, 10.7, and 14.6. address the WKB approximation, the coherent states, and the forced harmonic oscillator, respectively.

[38] H. F. Trotter, On the product of semi-groups of operators, Proc. Am. Math. Soc. **10**, 545 (1959).

[39] M. Suzuki, Generalized Trotter's formula and systematic approximants of exponential operators and inner derivations with applications to many-body problems, Commun. Math. Phys. **51**, 183 (1976).

[40] Farhi, J. Goldstone, S. Gutmann, J. Lapan, A. Lundgren, and D. Preda, A quantum adiabatic evolution algorithm applied to random instances of an NP-complete problem, Science **292**, 472 (2001).

[41] S. Wiesner, Simulations of many-body quantum systems by a quantum computer, arXiv:quant-ph/9603028.

[42] C. Zalka, Simulating quantum systems on a quantum computer, Proc. R. Soc. London A **454**, 313 (1998).

[43] A. Barenco, C. H. Bennett, R. Cleve, D. P. DiVincenzo, N. Margolus, P. Shor, T. Sleator, J. A. Smolin, and H. Weinfurter, Elementary gates for quantum computation, Phys. Rev. A **52**, 3457 (1995).

[44] M. Mottonen and J. J. Vartiainen, *Trends in Quantum Computing Research*, Decompositions of general quantum gates (NOVA Publishers, New York, 2006), Chap. 7.

[45] Likely, an optimal implementation of the phase factor $\exp(-i\theta E_v)$ can be achieved without using ancilla qubits.

[46] L. A. Wu, M. S. Byrd, and D. A. Lidar, Polynomial-Time Simulation of Pairing Models on a Quantum Computer, Phys. Rev. Lett. **89**, 057904 (2002).

[47] A. Kitaev and W. A. Webb, Wavefunction preparation and resampling using a quantum computer, arXiv:0801.0342.

[48] L. K. Grover, T. Rudolph, Creating superpositions that correspond to efficiently integrable probability distributions, arXiv:quant-ph/0208112.

[49] J. C. Spall, An Overview of the Simultaneous Perturbation Method for Efficient Optimization, Johns Hopkins APL Tech. Dig. **19-4**, 482 (1998).

[50] G. Wellein and H. Fehske, Self-trapping problem of electrons or excitons in one dimension, Phys. Rev. B **58**, 6208 (1998).

[51] J. B. Kogut and L. Susskind, Hamiltonian formulation of Wilson's lattice gauge theories, Phys. Rev. D **11**, 395 (1975).

[52] T. Byrnes and Y. Yamamoto, Simulating lattice gauge theories on a quantum computer, Phys. Rev. A **73**, 022328 (2006).

[53] E. Zohar, J. I. Cirac, and B. Reznik, Cold-Atom Quantum Simulator for SU(2) Yang-Mills Lattice Gauge Theory, Phys. Rev. Lett. **110**, 125304 (2013).

[54] K. E. Cahill and R. J. Glauber, Ordered expansions in boson amplitude operators, Phys. Rev. **177**, 1857 (1969).

[55] F. A. M. de Oliveira, M. S. Kim, P. L. Knight, and V. Buzek, Properties of displaced number states, Phys. Rev. A **41**, 2645 (1990).